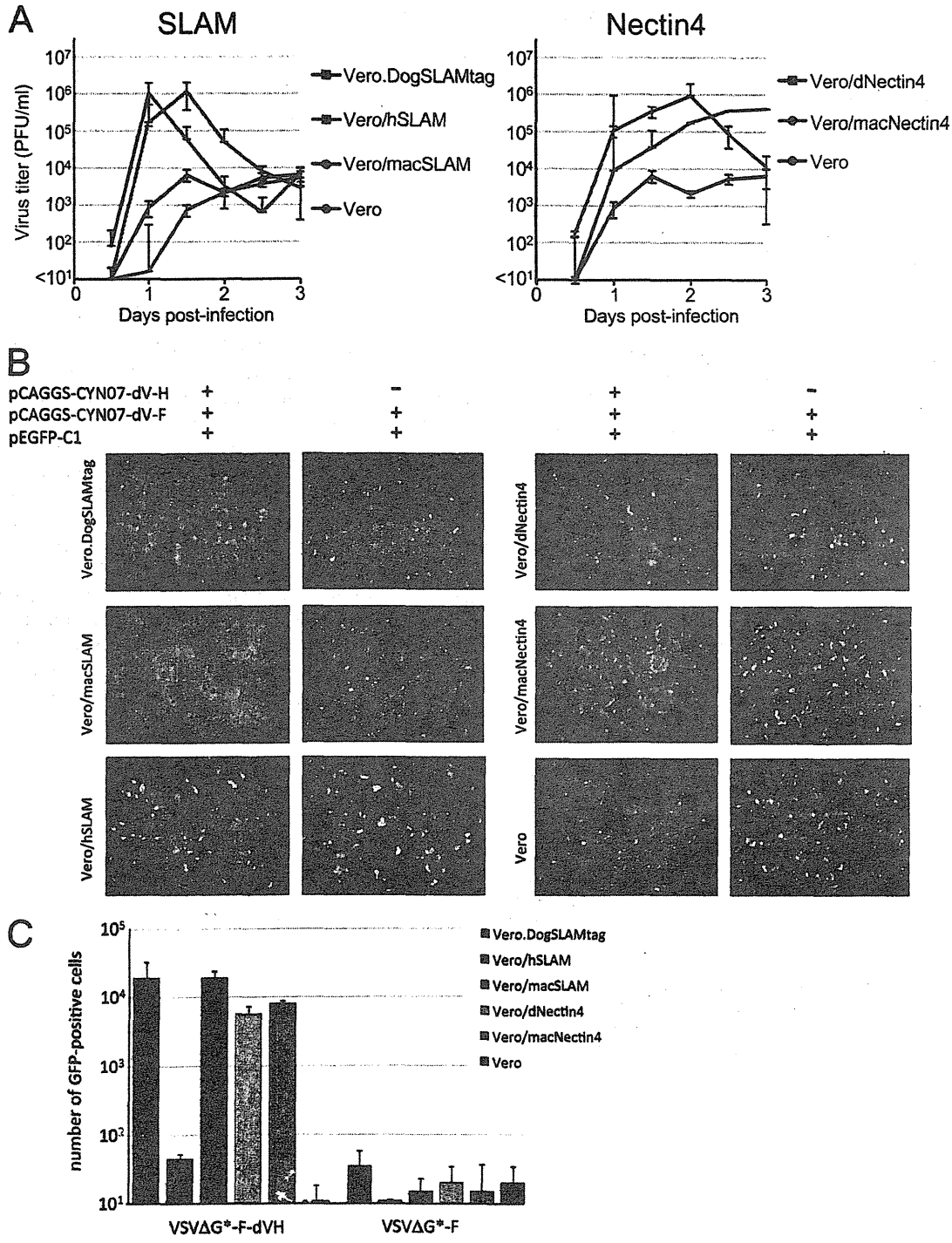

FIG 6 CYN07-dV utilizes macaca SLAM and macaca nectin4 as receptors. (A) Growth kinetics of CYN07-dV in Vero.DogSLAMtag, Vero/hSLAM, Vero/macSLAM, Vero/dNectin4, Vero/macNectin4, and Vero cells. The cells were infected with the virus at an MOI of 0.01, and titers at the indicated points were shown. (B) Induction of syncytium upon transfection with a mixture of plasmids expressing enhanced green fluorescent protein (EGFP) and CDV F with or without a plasmid expressing CDV H. (C) Infectivity of VSV pseudotype bearing H and F proteins of CYN07-dV (VSVΔG*-F-dVH) or that bearing the F protein (VSVΔG*-F) in Vero.DogSLAMtag, Vero/hSLAM, Vero/macSLAM, Vero/dNectin4, Vero/macNectin4, and Vero cells.

a sick dog, also replicated in the Vero/macSLAM cells; however, the appearance of syncytia was delayed in the Vero/macSLAM cells compared with that in the Vero.DogSLAMtag cells, and the peak titer of the virus in the Vero/macSLAM cells was significantly lower than that in the Vero.DogSLAMtag cells (data not shown).

To clarify whether the H and the F proteins of the virus induce syncytia in the cells expressing either SLAM or nectin4, cell-to-cell

fusion assay was performed upon transfection of the plasmids expressing the F and the H proteins of CYN07-dV. No syncytium formation was detected when the F protein of CYN07-dV alone was expressed in the cells (data not shown). On the other hand, many syncytia were observed in Vero.DogSLAMtag, Vero/macSLAM, Vero/dNectin4, and Vero/macNectin4 cells, but not in Vero and Vero/hSLAM cells, when the F and the H protein of CYN07-dV were expressed together (Fig. 6B). The syncytium formation was most remarkable in Vero/macSLAM cells (Fig. 6B). Although syncytia in nectin4-expressing Vero cells (Vero/dNectin4 and Vero/macNectin4) were smaller than those in SLAM-expressing cells (Vero.DogSLAMtag and Vero/macSLAM), syncytia in Vero/macNectin4 and Vero/dNectin4 cells were comparable (Fig. 6B).

To clarify the function of the H and the F proteins on entry of the virus via the SLAM and the nectin4, the infectivities of the VSV pseudotype bearing the H and the F protein of CYN07-dV, VSVΔG*-F-dVH, in various cells were compared. The VSV pseudotype bearing the F protein alone, VSVΔG*-F, did not infect any cells tested, whereas the VSVΔG*-F-dVH efficiently infected Vero/macSLAM cells and Vero.DogSLAMtag cells (Fig. 6C) but did not infect Vero/hSLAM cells. The VSVΔG*-F-dVH also efficiently infected Vero/macNectin4 cells and Vero/dNectin4 cells (Fig. 6C). These data showed that the CYN07-dV H protein efficiently utilizes macaca SLAM and macaca nectin4 as receptors.

DISCUSSION

Viruses in the genus *Morbillivirus* often cause severe diseases in animals and humans. Generally, symptomatic infection with each morbillivirus occurs in specific animal species or humans. Among the morbilliviruses, MV is the one that causes an acute febrile and systemic infection in humans. Although CDV also shows host specificity and causes acute infections primarily in dogs, it often affects animals in different species, including nonhuman primates, showing a high mortality rate. In the CDV outbreak that occurred among Japanese monkeys in Japan in 1989, only one monkey out of 34 died (14). However, in recent outbreaks in China and Japan, higher mortality rates were recorded: 4,250 monkeys out of ~10,000 died in Guangxi Province in 2006, 12 out of 20 died in Beijing in 2008, and 46 out of 432 died in Japan in 2008. Most authorized animal suppliers in China receive monkeys from a Guangxi farm and distribute monkeys to researchers throughout the mainland of China. Laboratory investigations of clinical specimens from moribund and/or dead monkeys in the present study and in earlier studies (15, 16) fulfilled the two criteria of Koch's postulates: (i) detection of CDV in sick animals and (ii) isolation of CDV in cultured cells. The experimental infection in the study further fulfill the remaining postulates: (iii) induction of a comparable disease in the original host and (iv) reisolation of CDV from experimentally infected animals. These findings proved that CDV is the primary cause of the outbreak in monkeys. Moreover, the numbers of monkeys infected with CDV in the Guangxi farm decreased greatly after the introduction of attenuated CDV vaccination in early 2009, even though a few cases have still been reported every year (15).

In the present study, mortality was not observed in experimentally CDV-infected monkeys. However, many monkeys, especially those that eventually became CDV antibody-positive at the outbreak, showed mild or no symptoms. Severe symptoms were observed only in some moribund and dead monkeys in the outbreak. Thus, mortality might have been observed if more monkeys were experimentally infected, even though we could not rule out the possibility of enhanced pathogenicity of CDV by coinfection of some other agent during the outbreak. To date, no other particular agents were detected in the monkeys. However, we could not rule out the possibility that isolation and passage of the virus in Vero/dog.SLAM could have caused a partial attenuation of the virus. This may be clarified in future to analyze the quasispecies of genome sequences of the virus in the original clinical samples of the monkey and to compare them to the sequence of the isolated virus.

In the present study, three moribund monkeys in the 2008 CDV outbreak showed upregulated levels of proinflammatory cytokines and chemokines, such as IL-1β, IL-6, MIP-1α, MIP-1β, MCP-1, eotaxin, IFN-γ, and IL-15. Anti-inflammatory responses of IL-1ra were also upregulated. In the rhesus monkeys infected with measles virus, suppression of IL-12 in the sera was reported (20). The induction of IFN-γ, IL-2, and MCP-1 in the sera of the measles virus-infected cynomolgus monkeys was also reported (21). However, comparable levels of upregulation in proinflammatory cytokines, chemokines, and anti-inflammatory responses of IL-1 receptor antagonist observed in the CDV-infected monkeys were not reported for the measles virus-infected monkeys. These observations are rather similar to rhesus monkeys infected with a lethal dose of Zaire ebolavirus (22). The mixed anti-inflammatory response syndrome in Zaire ebolavirus-infected monkeys is characterized by highly elevated levels of IL-13 and IL-1ra, which are similar to the CDV-infected monkeys in the outbreak. Thus, unbalanced responses of cytokines and chemokines may have contributed to the pathogenesis of fatal cases of CDV infection in monkeys in the outbreak.

The CYN07-dV efficiently infected Vero cells expressing dog and macaca SLAM but not the cells expressing human SLAM. This was confirmed by syncytium induction upon transient expression of the H and the F proteins of the virus and also by infectivity of the VSV pseudotype bearing the H and the F proteins of the virus. On the other hand, the CYN07-dV efficiently utilized nectin4 of dog and macaca. Thus, the CYN07-dV is capable of utilizing macaca SLAM and macaca nectin4 as receptors, as efficiently as dog SLAM and dog nectin4, respectively. These findings were consistent with the experimental infection of the CYN07-dV to cynomolgus monkeys, in which the virus infected PBMCs and epithelial cells expressing macaca SLAM and nectin4, respectively. Interestingly, the CYN07-dV did not efficiently utilize human SLAM as a receptor even though the SLAMs of human and macaca are highly conserved. Thus, at the moment, CDVs like CYN07-dV may not be a direct threat to humans. However, the expansion of host animal species of CDV to include primates might be a global threat in the future. Wild-type CDV strains isolated from dogs with distemper were recently shown to efficiently utilize both dog SLAM and dog nectin4 as receptors (13, 17). However, the wild-type CDV strain Ac96I also replicated in the Vero/macSLAM cells even though less efficiently than in the Vero.DogSLAMtag cells. This suggested that some wild-type CDV strain is capable of utilizing macaca SLAM as a receptor *per se*, even though the CYN07-dV utilizes macaca SLAM more efficiently. Thus, the CYN07-dV is considered to be adapted to spread among monkeys using macaca SLAM and macaca nectin4.

Nucleotide and amino acid sequence accession numbers. The complete nucleotide sequence of the CYN07-dV has been

deposited in DDBJ/GenBank under accession number AB687720, while the amino acid sequence of hemagglutinin protein has been deposited in DDBJ/GenBank under accession number BAM15593. The complete nucleotide sequences of mRNAs of cynomolgus monkey SLAM, pig-tailed monkey SLAM, and cynomolgus monkey nectin4 have been deposited in DDBJ/GenBank under accession numbers AB742520, AB742521, and AB742522, respectively.

ACKNOWLEDGMENTS

We thank Yusuke Yanagi for providing Vero.DogSLAMtag and Vero/hSLAM cells.

This work was supported in part by grants-in-aid from the Ministry of Health, Labor, and Welfare of Japan (grants H22-shinkou-ippan-006 and H24-kokui-shitei-003) and KAKENHI [Grant-in-Aid for Young Scientists (B), 22700459] from the Japan Society for the Promotion of Science (http://www.jsps.go.jp/english/).

REFERENCES

1. Kotani T, Jyo M, Odagiri Y, Sakakibara Y, Horiuchi T. 1989. Canine distemper virus infection in lesser pandas (*Ailurus fulgens*). Nihon Juigaku Zasshi. 51:1263–1266.
2. Perpiñán D, Ramis A, Tomás A, Carpintero E, Bargalló F. 2008. Outbreak of canine distemper in domestic ferrets (*Mustela putorius furo*). Vet. Rec. 163:246–250.
3. Hirama K, Goto Y, Uema M, Endo Y, Miura R, Kai C. 2004. Phylogenetic analysis of the hemagglutinin (H) gene of canine distemper viruses isolated from wild masked palm civets (*Paguma larvata*). J. Vet. Med. Sci. 66:1575–1578.
4. Hur K, Bae JS, Choi JH, Kim JH, Kwon SW, Lee KW, Kim DY. 1999. Canine distemper virus infection in binturongs (*Arctictis binturong*). J. Comp. Pathol. 121:295–299.
5. Roscoe DE. 1993. Epizootiology of canine distemper in New Jersey raccoons. J. Wildl. Dis. 29:390–395.
6. Osterhaus AD, Groen J, De Vries P, UytdeHaag FG, Klingeborn B, Zarnke R. 1988. Canine distemper virus in seals. Nature 335:403–404.
7. Appel MJ, Yates RA, Foley GL, Bernstein JJ, Santinelli S, Spelman LH, Miller LD, Arp LH, Anderson M, Barr M, Pearce-Kelling S, Summers BA. 1994. Canine distemper epizootic in lions, tigers, and leopards in North America. J. Vet. Diagn. Invest. 6:277–288.
8. Roelke-Parker ME, Munson L, Packer C, Kock R, Cleaveland S, Carpenter M, O'Brien SJ, Pospischil A, Hofmann-Lehmann R, Lutz H, Mwamengele GL, Mgasa MN, Machange GA, Summers BA, Appel MJ. 1996. A canine distemper virus epidemic in Serengeti lions (*Panthera leo*). Nature 379:441–445.
9. Robert AL, Griffith DP. 2007. Paramyxoviridae, p 1449–1496. *In* Fields BN, Knipe DM, Howley PM, Griffin DE, Lamb RA, Martin MA, Roizman B, Straus SE (ed), Fields virology, fifth ed. Lippincott-Raven, Philadelphia, PA.
10. Tatsuo H, Ono N, Yanagi Y. 2001. Morbilliviruses use signaling lymphocyte activation molecules (CD150) as cellular receptors. J. Virol. 75:5842–5850.
11. Mühlebach MD, Mateo M, Sinn PL, Prüfer S, Uhlig KM, Leonard VH, Navaratnarajah CK, Frenzke M, Wong XX, Sawatsky B, Ramachandran S, McCray PB, Jr, Cichutek K, von Messling V, Lopez M, Cattaneo R. 2011. Adherens junction protein nectin-4 is the epithelial receptor for measles virus. Nature 480:530–533.
12. Noyce RS, Bondre DG, Ha MN, Lin LT, Sisson G, Tsao MS, Richardson CD. 2011. Tumor cell marker PVRL4 (nectin 4) is an epithelial cell receptor for measles virus. PLoS Pathog. 7:e1002240. doi:10.1371/journal.ppat.1002240.
13. Pratakpiriya W, Seki F, Otsuki N, Sakai K, Fukuhara H, Katamoto H, Hirai T, Maenaka K, Techangamsuwan S, Lan NT, Takeda M, Yamaguchi R. 2012. Nectin4 is an epithelial cell receptor for canine distemper virus and involved in the neurovirulence. J. Virol. 86:10207–10210.
14. Yoshikawa Y, Ochikubo F, Matsubara Y, Tsuruoka H, Ishii M, Shirota K, Nomura Y, Sugiyama M, Yamanouchi K. 1989. Natural infection with canine distemper virus in a Japanese monkey (*Macaca fuscata*). Vet. Microbiol. 20:193–205.
15. Qiu W, Zheng Y, Zhang S, Fan Q, Liu H, Zhang F, Wang W, Liao G, Hu R. 2011. Canine distemper outbreak in rhesus monkeys, China. Emerg. Infect. Dis. 17:1541–1543.
16. Sun Z, Li A, Ye H, Shi Y, Hu Z, Zeng L. 2010. Natural infection with canine distemper virus in hand-feeding Rhesus monkeys in China. Vet. Microbiol. 141:374–378.
17. Seki F, Ono N, Yamaguchi R, Yanagi Y. 2003. Efficient isolation of wild strains of canine distemper virus in Vero cells expressing canine SLAM (CD150) and their adaptability to marmoset B95a cells. J. Virol. 77:9943–9950.
18. Niwa H, Yamamura K, Miyazaki J. 1991. Efficient selection for high-expression transfectants with a novel eukaryotic vector. Gene 108:193–199.
19. Tamura K, Dudley J, Nei M, Kumar S. 2007. MEGA4: molecular evolutionary genetics analysis (MEGA) software version 4.0. Mol. Biol. Evol. 24:1596–1599.
20. Griffin DE, Ward BJ, Jauregui E, Johnson RT, Vaisberg A. 1990. Immune activation during measles: interferon-gamma and neopterin in plasma and cerebrospinal fluid in complicated and uncomplicated disease. J. Infect. Dis. 161:449–453.
21. Takeuchi K, Nagata N, Kato SI, Ami Y, Suzaki Y, Suzuki T, Sato Y, Tsunetsugu-Yokota Y, Mori K, Van Nguyen N, Kimura H, Nagata K. 2012. Wild-type measles virus with the hemagglutinin protein of the Edmonston vaccine strain retains wild-type tropism in macaques. J. Virol. 86:3027–3037.
22. Ebihara H, Rockx B, Marzi A, Feldmann F, Haddock E, Brining D, LaCasse RA, Gardner D, Feldmann H. 2011. Host response dynamics following lethal infection of rhesus macaques with Zaire ebolavirus. J. Infect. Dis. 204(Suppl 3):S991–S999.

Triggering the measles virus membrane fusion machinery

Melinda A. Brindley[a], Makoto Takeda[b], Philippe Plattet[c], and Richard K. Plemper[a,d,1]

[a]Department of Pediatrics, Emory University School of Medicine, Atlanta, GA 30322; [b]Department of Virology III, National Institute of Infectious Diseases, Tokyo 208-0011, Musashimurayama, Japan; [c]Neurovirology Unit, Division of Experimental Clinical Research, Department of Clinical Research and Veterinary Public Health of the Vetsuisse Faculty, University of Bern, CH-3012 Bern, Switzerland; and [d]Children's Healthcare of Atlanta, Atlanta, GA 30322

Edited by Robert A. Lamb, Northwestern University, Evanston, IL, and approved September 12, 2012 (received for review June 27, 2012)

Paramyxoviruses contain glycoprotein fusion machineries that mediate membrane merger for infection. The molecular framework and mechanistic principles governing receptor-induced triggering of the machinery remain unknown. Using measles virus (MeV) fusion complexes, we demonstrate that receptor binding to only one dimer of the tetrameric attachment protein (H) dimer-of-dimers induces fusion-protein (F) triggering; receptor binding and F triggering can be communicated across the dimer–dimer interface of H; and the physical integrity of the tetramer is maintained during fusion. The central MeV H ectodomain stalk region requires structural flexibility for activation of F, and alanine substitutions in this section, physical stress, or exposure of H to soluble ligands trigger conformational rearrangements in native H tetramers. Binding of soluble receptor to H is sufficient to initiate refolding of F, underscoring the physiological significance of this rearrangement of the H tetramer. These data outline a model of the triggering of the physiological MeV fusion machinery in which unilateral receptor binding to one dimer pair in the H tetramer is sufficient to induce a reorganization of H that affects the conformation of the central stalk section, severing interactions between H and the F trimer and activating refolding of F.

paramyxovirus entry | protein refolding | virus envelope glycoproteins

Enveloped viruses display highly specialized glycoprotein fusion machineries, which, when activated, undergo a series of conformational changes ultimately resulting in membrane merger, fusion pore formation, and infection. All pathogens of the *Paramyxovirinae* subfamily depend on the concerted action of two glycoprotein complexes for infection; the attachment protein (H) binds to the cellular receptor and then activates refolding of the fusion protein (F), which facilitates membrane merger (1). Both proteins are thought to interact specifically in hetero-oligomeric fusion complexes (2–7).

Structural and biochemical studies have advanced our insight into conformational changes in F that are required for fusion (1). In contrast, basic questions about the molecular framework that defines productive receptor binding and the mechanism that links receptor binding to F triggering remain unaddressed: i.e., what is the minimal productive receptor:attachment protein stoichiometry; is receptor immobilization in the target membrane required for triggering of the paramyxovirus fusion machinery; does receptor binding affect the conformation of the attachment protein oligomer, and, if so, is this reorganization of the H tetramer instrumental for F triggering?

Measles virus (MeV), a representative of the *Morbillivirus* genus within the *Paramyxovirinae*, is a paramyxovirus archetype of high clinical significance. We have demonstrated that a homotetramer or higher-order multimer constitutes the physiological oligomer of the MeV H protein (8). Subsequent crystallization of the isolated globular head domains of MeV H complexed with soluble signaling lymphocyte activation molecule (SLAM/CD150) receptor has corroborated this view (9). Like all other *Paramyxovirinae* attachment proteins, the head domain of each MeV H monomer harbors receptor-binding sites (RBS) and assumes the classical β-barrel fold of sialidases, although the H protein lacks neuraminidase activity (9–12). A long stalk domain connects the head of the H protein to the transmembrane domain and short luminal tail. The binding sites for all three reported MeV receptors, CD46, SLAM, and nectin-4 (9, 11, 13), are located in an overlapping area of the head domain (14). MeV H and F complexes are thought to preassemble intracellularly (15), and discrete H stalk residues have been implicated in mediating F protein binding and triggering. Through biochemical analyses of full-length native MeV H fusion complexes, we have identified residues in the central section of the stalk domain (position 111–118) that, when mutated, prevent physical association of H and F. Position 98 in the H stalk, slightly more membrane proximal, was shown to be required for efficient triggering of F (16). Having developed an MeV H bimolecular complementation (H-BiC) assay, we furthermore demonstrated that the RBS, F-interacting, and F-triggering functionalities are truly distinct. Coexpression of H mutants with functional defects in these domains restores fusion-support activity through transcomplementation (8, 17).

The structure of the attachment protein stalk domains remains to be solved in its entirety, but the crystal structures of soluble Newcastle disease virus (NDV) hemagglutinin-neuraminidase (HN) attachment protein head and partial stalk domains show a four-helix bundle (4HB) organization of the stalk (18). This arrangement was corroborated by the structure of the parainfluenza virus type 5 (PIV5) HN stalk (19), suggesting that a 4HB stalk arrangement is conserved among *Paramyxovirinae* attachment proteins.

Crystal structures of free and receptor-bound isolated H head domains in monomeric, dimeric, or tetrameric configurations have revealed that the fold of individual head monomers and the organization of the monomer–monomer interface in covalently linked H dimers remain largely unchanged upon receptor binding (9–12). By contrast, tetrameric ectodomain fragments of both H- (9) and related HN-type (18, 20) attachment proteins crystallized in different spatial organizations. For H, these structures were speculated to represent pre- and postreceptor bound/F-triggering conformations. However, the physiological relevance of individual conformations of purified H ectodomain fragments and the question of whether receptor binding induces a reorganization of the attachment protein remain unaddressed.

Building on available structural and functional information and using an array of newly established functional assays, the present study identifies fundamental determinants that link H

Author contributions: M.A.B. and R.K.P. designed research; M.A.B. and R.K.P. performed research; M.A.B., M.T., P.P., and R.K.P. contributed new reagents/analytic tools; M.A.B., M.T., P.P., and R.K.P. analyzed data; and M.A.B. and R.K.P. wrote the paper.

The authors declare no conflict of interest.

This article is a PNAS Direct Submission.

[1]To whom correspondence should be addressed. E-mail: rplempe@emory.edu.

See Author Summary on page 17750 (volume 109, number 44).

This article contains supporting information online at www.pnas.org/lookup/suppl/doi:10.1073/pnas.1210925109/-/DCSupplemental.

receptor engagement to F triggering. Cysteine engineering combined with the H-BiC assay defined the molecular framework of H tetramer–receptor interactions that are necessary for fusion triggering. Insertion of disulfide bonds at strategic positions probed the physiological relevance of existing structural models of the H tetramer, and biochemical and functional assays explored the effect of soluble and membrane-embedded receptor on the H tetramer and associated F trimer organization under physiological conditions.

Results

We have shown previously that bioactivity of MeV H mutants with discrete functional defects (illustrated in Fig. 1*A*) can be restored through protein transcomplementation after coexpression (8). This H-BiC assay provides a platform to explore individual H functionalities in the context of physiological, membrane-embedded fusion complexes. However, the approach is limited by an inherent inability to differentiate between complementation on a heterodimer or [which presumably would be more informative based on recent structural information (9)] on a homodimer/heterotetramer level. To explore transcomplementation across the dimer–dimer interface in H homodimer/heterotetramers complementation pairs, we hypothesized that the two natural disulfide bonds at H stalk positions 139 and 154, which mediate covalent H dimerization, could be used in a combination of H-BiC with disulfide bond engineering (Fig. 1*B*).

MeV H Heterodimers with Unpaired Stalk Thiols Are Intracellularly Retained. Previously, we have demonstrated that substituting either cysteine 139 or cysteine 154 with serine retains H bioactivity (21). We therefore anticipated that coexpression of standard H with H-C139S will result in the formation of H-H and (H-C139S)-(H-C139S) homodimers that are fully intracellularly transport competent because of the pairing of all reactive thiol moieties present in the ectodomains. In contrast, H-(H-C139S) heterodimers are expected to be intracellularly retained by endoplasmic reticulum (ER)-resident isomerases that target unpaired, reactive thiol groups (22). H variants harboring HA or Flag epitope tags for distinction were generated to test this hypothesis conceptually in coimmunoprecipitation experiments of cell-surface–exposed and total H material.

H_{HA}-H_{FLAG} complexes were present in both whole-cell extracts and the plasma membrane fractions. However, plasma membrane levels of H_{HA}-(H-C139S_{FLAG}) heterodimers were greatly reduced (Fig. 1*C*), demonstrating that disulfide engineering is suitable to control the composition of H tetramers in surface-exposed, functional fusion complexes. Equivalent results were obtained with H variants featuring the C139S substitution in addition to one of the signature mutations of the different complementation groups, i.e., F111A, which affects F interaction (6); ΔCD46, which affects receptor binding (23, 24); or I98A, which affects F triggering; Fig. 1*C* (16).

Unilateral Receptor Engagement by a Single Dimer of the H Tetramer Is Sufficient for F Triggering. To explore whether transcomplementation of the individual H functionalities can be achieved in a homodimer/heterotetramer setting, we coexpressed H complementation variants pairwise in all combinations with MeV F and quantified bioactivity using a luciferase reporter-based cell-to-cell fusion assay. Efficient complementation, similar to that seen with the H-C139S reference, was observed upon combination of H-I98A-C139S with H-ΔCD46 (Fig. 2 and Fig. S1). In contrast, F-triggering activity was not restored when we paired F-interaction–deficient H-F111A homodimers with homodimers of either of the other two complementation groups. Naturally, the C139S substitution itself did not restore the triggering competence of any of the H mutants when expressed with F alone for control.

These results indicate that unilateral receptor binding to only one of the covalently linked dimer pairs in the attachment protein tetramer is sufficient for F triggering. Unlike efficient compensation of the H-F111A substitution in a heterodimer setting (8), however, F-binding–deficient H-F111A homodimers cannot be complemented *in trans*.

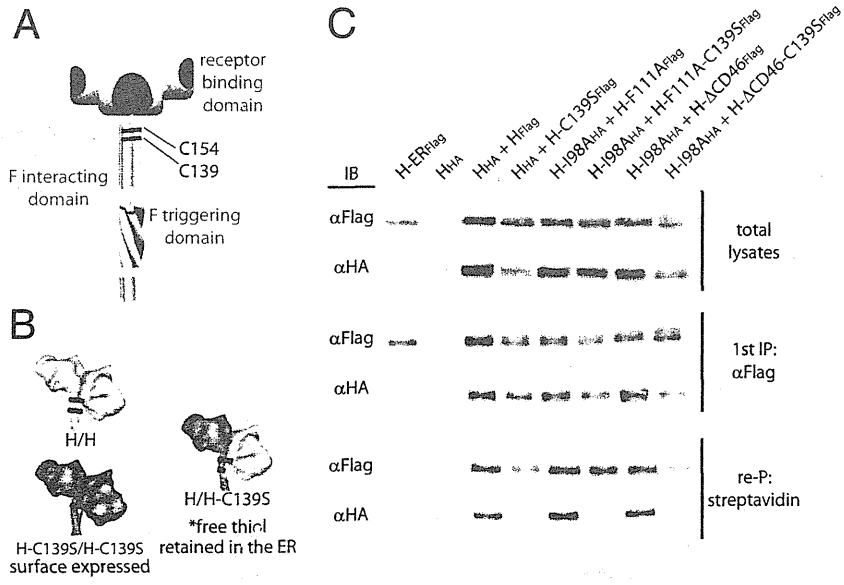

Fig. 1. Cysteine engineering to assess selective H transcomplementation on a homodimer/heterotetramer level. (*A*) Schematic of the MeV H tetramer; the locations of independent complementation groups and naturally present disulfide bonds are indicated. (*B*) Illustration of the cysteine-engineering strategy. (*C*) Coimmunoprecipitation of epitope-tagged surface-exposed H dimers confirms that only H homodimers with paired thiol moieties reach the cell surface. Surface proteins were biotinylated, and total cell lysates were subjected to α-Flag immunoprecipitation (first IP), followed by reprecipitation (re-P) of the plasma membrane fraction with immobilized streptavidin. A previously described H variant carrying an endoplasmic reticulum-retention signal (H-ER$_{Flag}$ (15)] served as specificity control for the streptavidin reprecipitation. Immunoblots were developed with α-Flag or α-HA antibodies, respectively.

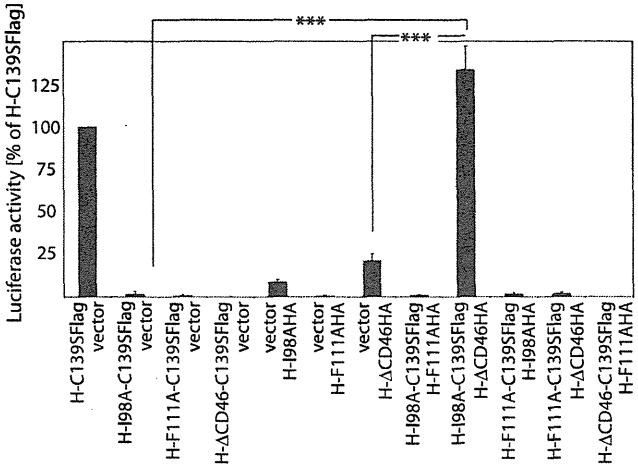

Fig. 2. Unilateral interaction of a receptor with a single covalently linked H dimer is sufficient to initiate F triggering. Results of a quantitative firefly luciferase-based cell-to-cell fusion assay assessing H transcomplementation are shown; data represent averages of at least four experiments ± SEM; ***$P < 0.001$.

Distinct Conformations of Attachment Protein Tetramers. Two distinct scenarios could account for this lack of trans-complementation: Heterotetramers containing H-F111A homodimers could form physically but lack functionality, suggesting that each covalent dimer pair must contain at least one F-binding–competent H monomer. Alternatively, H-F111A homodimers may be unable to associate into heterotetramers with either H-I98A or H-ΔCD46 homodimers, implying that they assume a conformation that is competent for intracellular transport but conformationally distinct from either H-I98A or H-ΔCD46.

To differentiate between these possibilities, we generated a set of electrophoretically distinct H variants by adding single-chain antibody moieties as size tags to the H C terminus as reported previously (25). Adding single or tandem copies of the single-chain antibody resulted in H_{XL} and H_{XXL} constructs, respectively, with an estimated increase of ~25 kDa per single-chain antibody copy, largely unchanged bioactivities (Table S1), but clearly distinguishable electrophoretic mobility (Fig. S2*A Upper*). Electrophoretic separation of surface-expressed material after coexpression of standard and size-tagged H constructs under denaturing, nonreducing conditions underscored that heterodimers form readily but that heterodimers harboring an unpaired thiol moiety at position 139 are not competent for intracellular transport (Fig. S2*A Lower*), confirming that the added single-chain domain does not affect the homodimer engineering strategy.

We next subjected the size-tagged H_{XXL} constructs to digitonin extraction followed by native-PAGE, which fractionates the intact H tetramers according to mass, shape, and surface charge (8, 26). When standard and size-tagged variants of otherwise unmodified H, H-I98A, and H-ΔCD46, all with and without the C139S substitution, were coexpressed, tetramers of intermediate mobility representing mixed homodimer/heterotetramers complexes became readily appreciable in addition to untagged and size-tagged homotetramers (Fig. 3*A*). However, H homodimers harboring the F111A mutation failed to engage in mixed tetramers with standard H, H-I98A, or H-ΔCD46-dimers (Fig. 3*A*), suggesting that H-F111A tetramers have a distinct conformation. Fig. S2*B* summarizes the complementation and oligomerization phenotypes of all H constructs analyzed in an activity matrix.

Under native-PAGE conditions, conformational rearrangements that result in a change of protein shape and/or surface charge typically are reflected by an altered mobility pattern (27, 28). Indeed, direct comparison of standard H and representatives of the different H complementation groups without additional size tags revealed two distinct banding patterns: tetramers of all H mutants that are confirmed to abrogate physical interaction with F [i.e., H-F111A, H-L114A, H-I118A, and an H-110–114A quintuple mutant (6)] were found predominantly in a fraction of higher electrophoretic mobility than those of standard H, F-triggering–, or receptor-binding–defective H variants (Fig. 3*B Upper*). A small fraction of H-F111A, H-L114A, and H-I118A found at higher molecular weight may represent higher-order oligomers or protein aggregates. Standard reducing and denaturing SDS/PAGE of the same samples confirmed that the underlying H monomers are all of equivalent molecular weight (Fig. 3*B Lower*). Because the overall protein pI is unaffected by the amino acid substitutions introduced at H positions 111, 114, or 118, the altered native-PAGE mobility pattern indicates a different conformation of the F-binding–deficient H tetramers that is distinct from that of standard H, H-I98A, and H-ΔCD46.

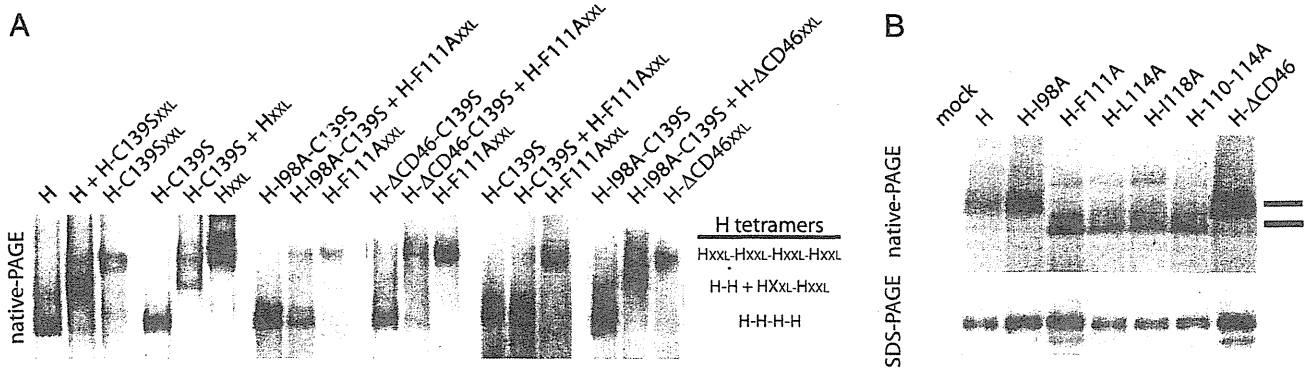

Fig. 3. H-F111A homodimers are structurally distinct from homodimers of unmodified H or other H-complementation groups. (*A*) Native-PAGE analysis of digitonin-extracted H tetramers reveals that H-F111A homodimers are unable to heterotetramerize with any other H homodimer species. To distinguish better untagged and size-tagged H oligomers in native-PAGE, size-increased H constructs contained a tandem copy of the tag H_{XXL}. The migration positions of size-tagged H homo- and heterotetramers are shown. (*B*) H homotetramers harboring stalk mutations that prevent interaction with F (F111A, L114A, I118A, or 110-114A) show a distinct migration pattern in native gels. The predominant H tetramer migration profiles of standard H, H-I98A, and H-ΔCD46 (gray marker) and H-F111A (black marker) are shown.

Induced Rearrangement of the H Tetramer into an H-F111A–Like Conformation. To test the physiological relevance of the different H tetramer organizations, we examined whether standard H tetramers can rearrange into an H-F111A–like conformation. We first explored the effect of increasing detergent stringency or temperature shock on the organization of H tetramers. n-Dodecyl β-D-maltoside (DDM) is, like digitonin, a nonionic detergent used for native-PAGE (26), but in our experience it applies higher scrutiny to larger protein complexes such as the MeV H tetramer (8). Adding increasing amounts of DDM to digitonin-extracted H tetramers reliably converted the standard H and H-I98A tetramer mobility pattern to the H-F111A profile (Fig. 4*A*). Consistent with our previous observations (8), H tetramers partially disintegrated into the covalently linked dimers at higher DDM concentrations.

Heat exposure has been used to trigger refolding of purified paramyxovirus F proteins into the postfusion conformation (29). When we subjected the MeV H complexes in an analogous experimental approach to brief (10-min) heat treatment followed by native-PAGE, we noted predominant reorganization of standard H and H-I98A tetramers into an H-F111A–like configuration at or above 50 °C (Fig. 4*B*), comparable to the conformational shift observed in the presence of increasing DDM concentrations.

Proteinaceous Ligands Induce H Tetramer Reorganization. To assess further the relevance of detergent or heat-induced H tetramer rearrangements, we next exposed the panel of H variants to purified, soluble SLAM receptor (sSLAM) (Fig. 5*A*) (6) or a neutralizing monoclonal antibody (mAb E128) that recognizes an epitope located in the CD46 RBS (Fig. 5*B Upper*), followed by digitonin extraction and native-PAGE. After the addition of sSLAM or RBS-specific mAb, the electrophoretic mobility of H oligomers was reduced, indicating the formation of larger H tetramer-sSLAM and H tetramer-mAb complexes. Importantly, the mobility profile of all three H variants (standard H, H-I98A, and H-F111A) became similar when complexed with sSLAM or RBS-specific mAb. In contrast, the difference in mobility between H-F111A and standard H or H-I98A remained when a nonneutralizing α-MeV H mAb mixture was added for comparison (Fig. 5*B Lower*). sSLAM and the different mAbs displayed similar electrophoretic mobility in native-PAGE when fractionated in the absence of H complexes (Fig. S3*A*), and an H-ΔCD46 variant that is not recognized by mAb E128 (Fig. S3*B*) confirmed the specificity of the mAb E128–H interaction (Fig. 5*B*).

To address whether gel shifts induced through physical stress (heat shock or stringent detergent extraction) and through the addition of protein ligands (sSLAM or α-RBS mAb) visualize equivalent rearrangements of the H tetramer, we examined the effect of heat shock and exposure to ligand in combination. If either procedure induced H tetramer rearrangements of the same molecular nature, we would expect to extract H complexes with mobility equal to that of complexes exposed to soluble ligand alone. This was indeed the case when gel shift assays were performed after consecutive exposure of standard H tetramers to heat and/or proteinaceous (sSLAM or mAb E128) ligands (Fig. 5*C*). These data indicate that standard H tetramers can rearrange into an H-F111A–like conformation and suggest that binding of proteinaceous ligands (either soluble receptor or RBS-specific mAbs) to H is sufficient to trigger this reorganization.

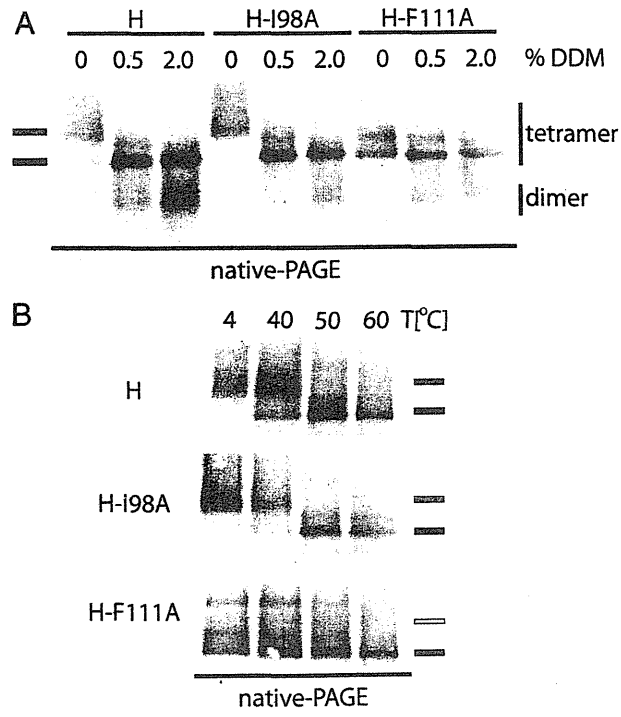

Fig. 4. Physical stress induces transition of H tetramers to an H-F111A–like conformation. (*A*) Digitonin extracts of H tetramers were treated with increasing amounts of DDM and subjected to native-PAGE fractionation. The predominant tetramer migration profiles as observed in Fig. 3*B* are shown. (*B*) Digitonin extracts of H tetramers were subjected to 10-min heat treatment before native-PAGE analysis.

Upper H Stalk Sections Retain a Closed Arrangement During F Triggering. Different conformations of H oligomers appear consistent with the two distinct tetrameric crystal structures that were reported recently for soluble MeV H head domains complexed with SLAM receptor (9). Of these, a predicted pre-F triggering conformation (form I) posits the H stalk domains in a 4HB arrangement, compatible with that observed in NDV and PIV5 HN stalk structures (18, 19). In contrast, a second structure (form II) that was suggested to represent a postreceptor-bound/F-triggering organization of the H tetramer features discrete H stalk dimers. The transition of H from form I to form II was predicted to coincide with the separation of the membrane-distal stalk sections (9).

Fig. 6*A* provides a homology model of the central MeV H stalk section that we generated based on the PIV5 HN coordinates. The model positions residues 98, involved in F triggering (16), and 111 flanking a predicted transition from a twisted to a straight 4HB arrangement. Based on the inability of H-F111A tetramers to interact with F, we considered that the higher H-F111A–like mobility may represent a form II-like structural organization. To test the relevance of form II experimentally, we inserted cysteine substitutions at selected positions along the length of the H stalk. The resulting H variants were assayed first for intracellular transport competence (Table S1) and the formation of covalently linked tetramers assessed through electrophoretic fractionation under reducing and nonreducing conditions (Fig. 6*B*). Two of the constructs, H-K72C and H-I122C, were not surface expressed, presumably because of the presence of unpaired thiol moieties in the stalk. Of the remaining, intracellular transport-competent mutants, four H variants (H-L114C, H-Y131C, H-D132C, and H-D151C) exist predominantly (>50%) as covalently linked tetramers (Fig. 6 *B* and *C*).

When we assessed the bioactivity of these constructs in quantitative fusion assays, no clear correlation between covalent H tetramerization and fusion-triggering activity was observed. The three H variants that showed the highest degree of covalent tetramers (H-Y131C, H-D132C, and H-D151C) were all capable of robust F triggering, ranging from ~60–120% of that found for standard H (Fig. 6*C*). These data indicate that the molecular integrity of preformed H tetramers is conserved during F triggering and reveal the consistently maintained close proximity of the

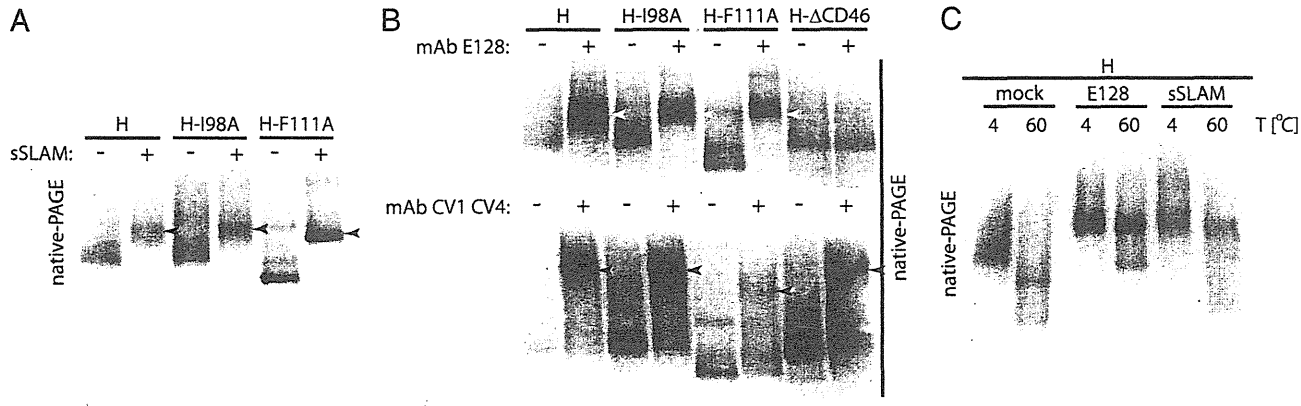

Fig. 5. RBS-specific soluble ligands induce H tetramer reorganization. (*A*) Exposure of H-expressing cells to sSLAM before digitonin extraction and native-PAGE analysis returns H tetramer/sSLAM complexes of similar mobility (arrowheads). (*B*) Exposure of H-expressing cells to RBS-specific mAb E128 (competes with CD46 receptor binding) or nonneutralizing H-specific mAbs CV1 CV4. Although all E128/H tetramer complexes show indistinguishable migration profiles (white arrowheads), CV1 CV4/H-F111A tetramers retain distinct electrophoretic mobility (black arrowheads). (*C*) Consecutive exposure of H tetramers to heat and RBS-specific ligands. H material was extracted with digitonin and was kept at 4 °C (4) or was heated to 60 °C (60) for 10 min. Subsequently, samples were exposed to RBS-specific ligand (E128, sSLAM) or vehicle (mock).

membrane-distal (upper) stalk sections in pre- and postreceptor-bound H complexes.

F Triggering Requires Structural Freedom in the Central Section of the H Stalk. If the F111A mutation indeed induces a postreceptor-bound–like organization of H, this finding implies that the conformation of H-F111A tetramers should be distinct from that of crystal form II. To test this notion, we examined whether H-F111A variants remain capable of forming covalently linked tetramers when cysteine substitutions are added to stalk positions membrane proximal or distal of the F111A site (i.e., positions L74C, Y131C, D132C, or D151C). Comparative analysis of

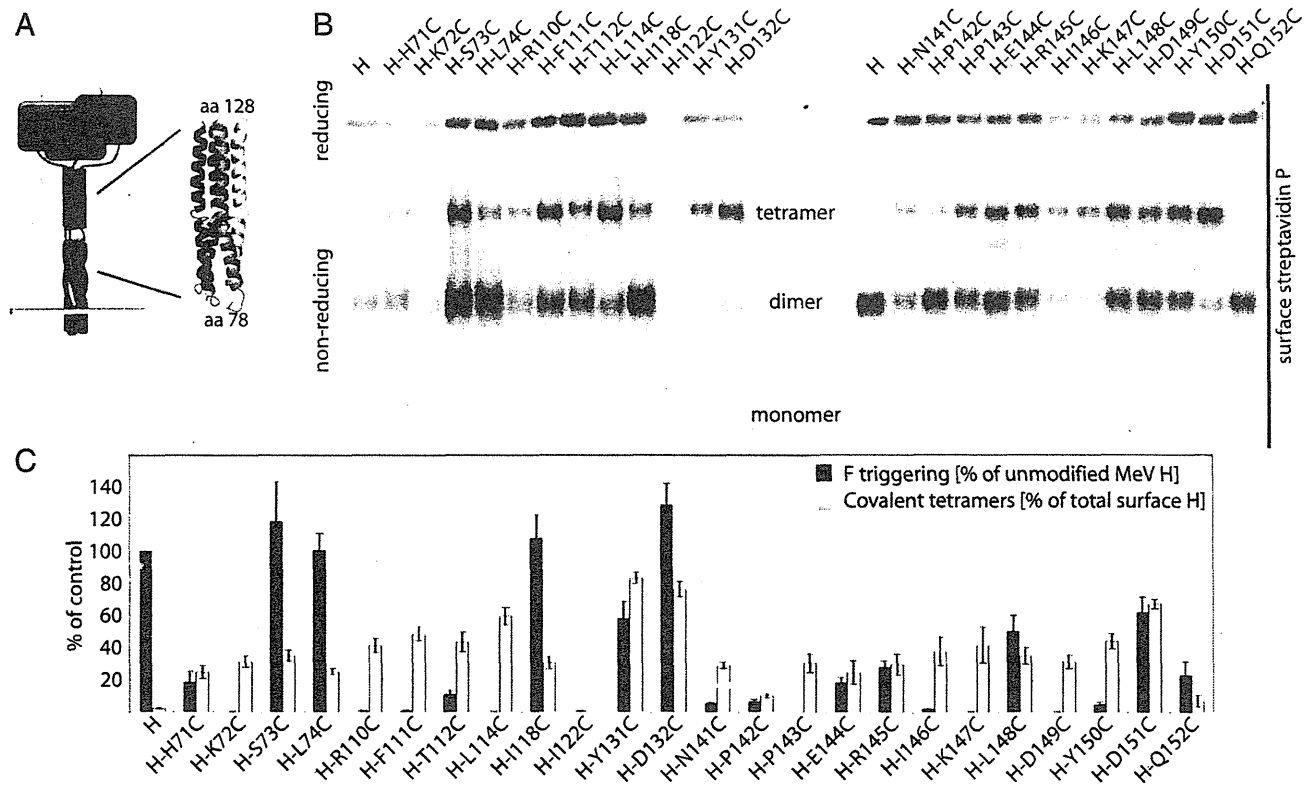

Fig. 6. Membrane-distal (upper) H stalk sections maintain close physical proximity during F triggering. (*A*) Overview of the cysteine-scanning mutagenesis performed along the H stalk, represented by a yellow bar (*Left*) in the cartoon. (*Inset*) Homology model of the central section of the MeV H stalk, generated in Swiss-MODEL based on the coordinates of a PIV5 HN stalk fragment (PDB ID 3TSI). (*B*) Assessment of the covalent oligomerization status of cell-surface–exposed H cysteine mutants under reducing and nonreducing conditions. (*C*) Quantitation of relative amounts of surface-exposed H in covalent tetramers (based on densitometric analysis of gels as shown in *B*) and F-triggering activity; data represent average of four experiments ± SEM.

these constructs with the corresponding single mutants under reducing and nonreducing conditions demonstrated that the F111A exchange does not affect the degree of covalent H tetramerization (Fig. 7*A*). Of note, combining distal cysteine insertions with removal of the naturally existing disulfide bonds at stalk positions 139 or 154 abrogates essentially all covalent H tetramerization (Fig. 7*B*), indicating that the natural disulfide bonds at positions 139 and 154 introduce a rigid scaffold into the dimeric stalk pairs that is required for covalent tetramerization.

In contrast to the high bioactivity of H tetramers with covalently rigidified upper-stalk sections, cysteine substitutions introduced into the central part of the stalk itself (residues 110, 111, 112, and 114) largely blocked F triggering (Figs. 6C and 7C). An exception was H-118C, which maintained efficient fusion support activity. Consistent with this finding, H-118C, but not H-118A, is able to associate efficiently with F (Fig. S4), underscoring the highly specific side-chain requirement in the H stalk section for productive F binding. However, when we partially released disulfide bonds of H-110C, H-111C, H-112C, and H-114C under mildly reducing conditions [25 mM dithiothreitol (DTT)], the bioactivity of all variants except H-114C was restored substantially, to ~60–85% of that observed for standard H (Fig. 7*C*). This finding is consistent with our recent analysis of the homologous region of the related canine distemper virus H protein (30), suggesting that structural, possibly rotational, freedom between stalk monomers in a central, but not upper, stalk section is a conserved requirement for morbillivirus F triggering. Although additional disulfide bonds near stalk position 111 arrest H-F111C tetramers in a reactivatable, pre–F-triggering organization, the conformation of H-F111A tetramers may represent a distinct postreceptor-bound/F-triggering form of the tetramer.

Exposure of H Tetramers to Soluble Receptor Initiates F Trimer Refolding. To test directly whether the H-F111A tetramer conformation represents a post-F-triggering form, we examined the effect of soluble receptor-induced H tetramer rearrangements on the initiation of F triggering in physiological, membrane-embedded fusion complexes. To detect the initiation of F trimer refolding, we used a pair of mAbs directed against the MeV F protein, mAb 186A (31) and, mAb 19GD (32), which we have found specifically detect a pretriggered (α-pre F) or a fusion-triggered (α-trig F) conformation of the F trimer, respectively (Fig. 8*A*).

To generate conditions void of high-affinity receptor stimulation of H, CD46-binding– incompetent H-ΔCD46 and F were coexpressed in Vero cells, which lack both SLAM and nectin-4 (9, 13) and therefore do not provide a receptor for H-ΔCD46. In this system, we observed strong reactivity of F trimers with the pretriggered F-specific mAb in cell-surface immunoprecipitation assays, whereas the corresponding α-triggered F-specific mAb showed little binding (Fig. 8*B*). Likewise, F expressed in the absence of H maintained full reactivity with the pretriggered F-specific mAb. These data indicate that prefusion MeV F trimers have a low rate of spontaneous refolding in the absence of H interaction with receptor and demonstrate that MeV F does not require physical contact with H to retain a metastable prefusion conformation.

When MeV glycoprotein-expressing cells were exposed to soluble SLAM, however, reactivity with the α-triggered F mAb increased substantially to levels comparable to those achieved through overlay with SLAM-positive Vero-SLAM cells, which served as a positive control for the assay (Fig. 8*B*). Corroborating previous reports that the I98A substitution in the H stalk impairs F triggering but not physical interaction between H and F complexes (8, 16), exposure of H-I98A tetramers to membrane-integral or soluble receptor in this experimental setting did not result in increased F reactivity with the α-triggered F mAb (Fig. S5*A*).

To explore whether the soluble SLAM-mediated initiation of F triggering is sufficient to drive the opening of fusion pores, we adapted a recently described real-time cell-content–mixing assay to the paramyxovirus system; this assay is based on the functional reconstitution of individually expressed N- and C-terminal halves of GFP/renilla luciferase dual-fusion proteins upon the formation of fusion pores (33). Monitoring the reconstitution of functional luciferase moieties in this setting revealed successful opening of fusion pores only in the presence of membrane-integral receptor (Fig. 8*C*). Low-level content mixing observed with the H-ΔCD46 and F combination in the absence of soluble SLAM is most likely caused by residual low-affinity docking of H-ΔCD46 to the CD46 receptor. Importantly, exposure of Vero cell populations expressing H-ΔCD46 and F to soluble SLAM did not

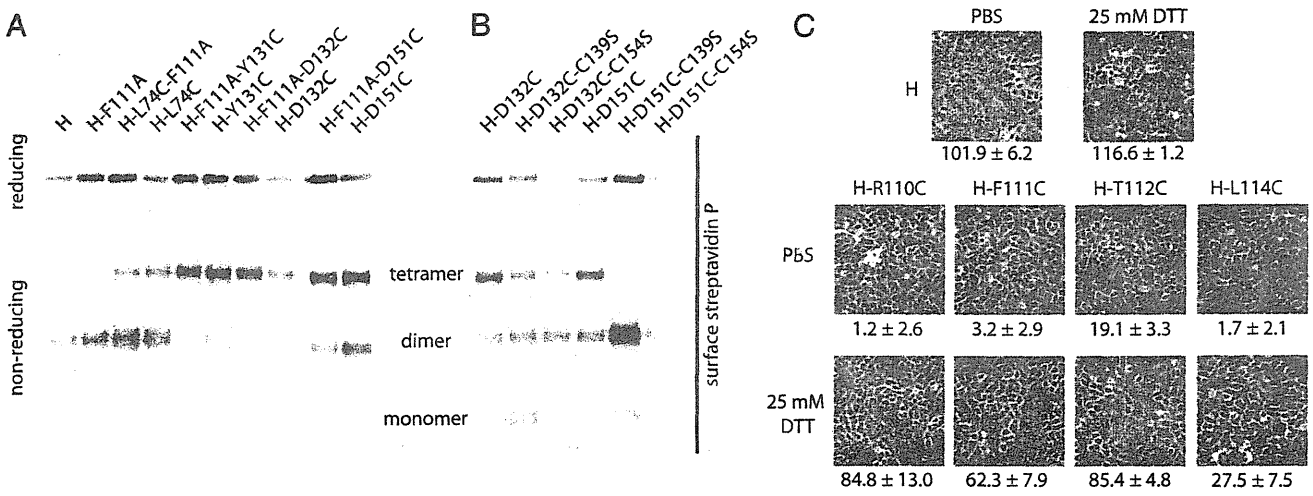

Fig. 7. Structural flexibility of the central section of the H-stalk domain is required for F triggering (*A* and *B*) Assessment of the covalent oligomerization status of selected H cysteine mutants. (*C*) Microphotographs of Vero cells coexpressing MeV H constructs with standard F protein. Before imaging, cells were exposed to mildly reducing conditions (25 mM DTT) or vehicle (PBS) for control. Numbers represent the amount of nuclei found in a syncytia/standardized field of view (each control field contains ~100–120 cells). Averages of 75 fields of view ± SEM are shown.

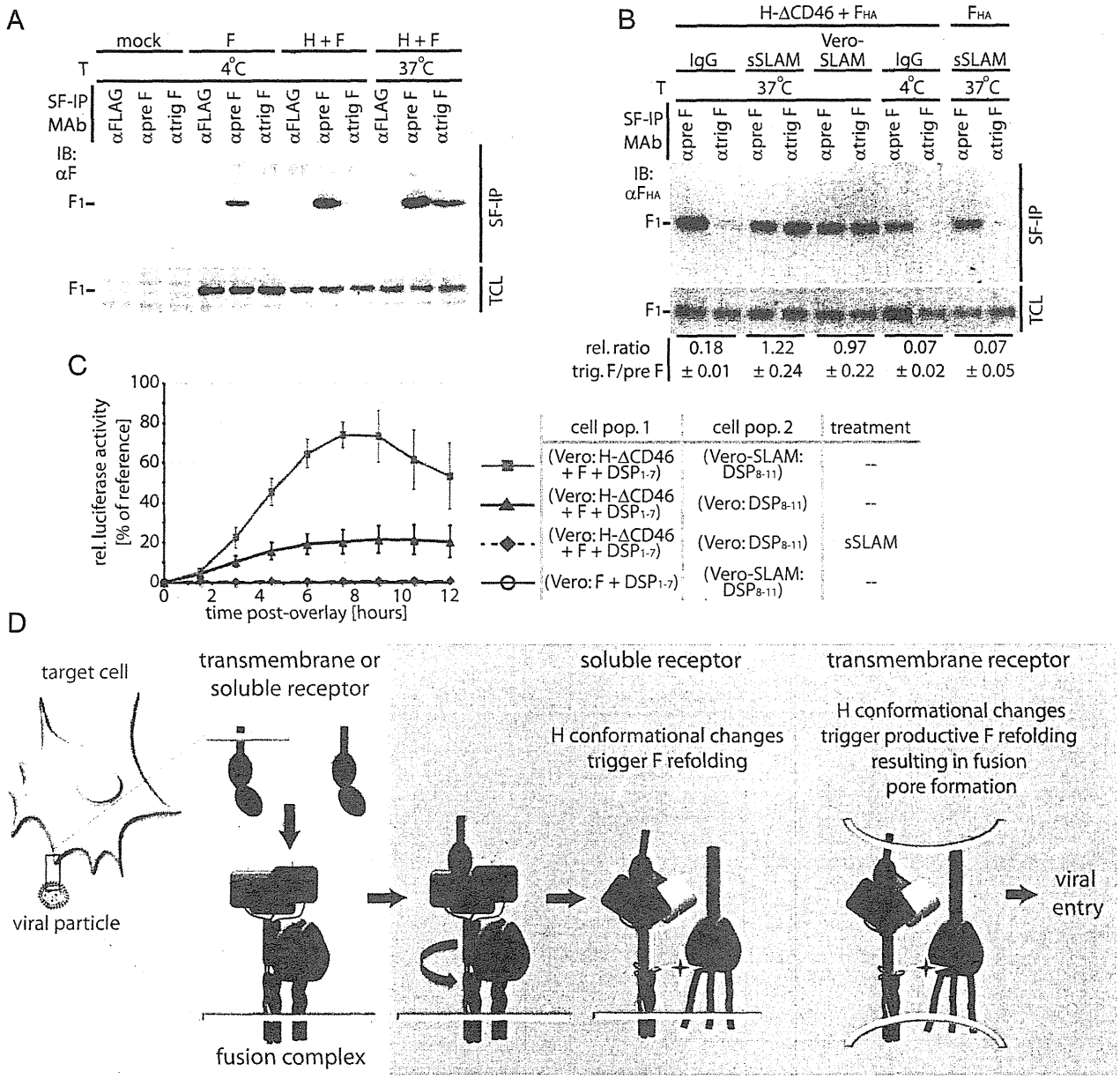

Fig. 8. H tetramer conformational changes induced by soluble receptor are sufficient to initiate F refolding. (*A*) Surface immunoprecipitation (SF-IP) of Vero cells coexpressing MeV H and F. Precipitation of F material with a conformation-dependent mAb that recognizes a fusion-triggered F trimer (αtrig F) requires warming of samples to 37 °C, allowing F refolding to proceed. A mAb recognizing prefusion F (αpre F), and a control mAb (αFlag) were used for comparison. (*B*) Surface immunoprecipitation of MeV F protein with conformation-dependent αpre F and αtrig F mAbs as specified. Overlay of MeV SLAM receptor-positive cells (Vero-SLAM) or sSLAM is sufficient to initiate F refolding. Numbers represent densitometric ratios of triggered F/prefusion F, normalized for F material present in total cell lysates (TCL); averages of three experiments ± SEM are shown. (*C*) Initiation of F refolding by soluble receptor does not lead to fusion pore formation. Values were normalized for cells cotransfected with DSP_{1-7} and DSP_{8-11} plasmids (33) and represent averages of four to six experiments ± SEM. (*D*) Model of the MeV fusion machinery. Contact of a single H dimer present in functional fusion hetero-oligomers (light blue background; H tetramers are colored by monomer; F trimers are in dark blue) with membrane-embedded or soluble receptor leads to reorganization of the central H stalk section (red arrow); this reorganization most likely coincides with rearrangements of the H head domain. This H tetramer reorganization triggers the F refolding cascade. However, interaction of H with membrane-embedded receptor is required for productive membrane fusion.

lead to increased cell content mixing and syncytia formation in this assay or upon microscopic examination (Fig. S5*B*).

These studies demonstrate that binding of soluble receptor molecules to a native, membrane-embedded paramyxovirus attachment protein oligomer is sufficient to activate the F refolding pathway, suggesting that the ligand-induced changes in H electrophoretic mobility in native gels reflect an H tetramer reorganization that constitutes the central link between binding to a receptor and triggering of the F fusion machinery. Opening of fusion pores, however, requires the presence of membrane-embedded receptor.

Discussion

Paramyxoviruses depend on the concerted action of two envelope glycoprotein complexes to achieve membrane fusion and infection. In this study, we subjected full-length, membrane-

integral MeV attachment protein complexes to an array of biochemical and functional assays to dissect the molecular mechanism that links receptor engagement by the H protein to F-triggering under physiological conditions.

From H transcomplementation assays (8) combined with cysteine-substitution–based homodimer engineering, we conclude, first, that an H monomer:receptor stoichiometry ≤2:1 initiates fusion and that unilateral receptor docking to only one of the covalently linked dimer pairs in the H tetramer is necessary and sufficient. Based on these results, we can exclude triggering models that assume separation of the tetrameric H head arrangement along the noncovalent dimer–dimer interface as a result of physical force generated through simultaneous binding of membrane-immobilized receptor molecules to each covalent dimer pair. However, productive complementation across cysteine-engineered F-triggering– or receptor-binding–defective H homodimers reveals functional cross-talk along the dimer–dimer interface.

The generation of triggering-competent covalently linked H tetramers through disulfide bond engineering into the upper (membrane-distal) stalk domain indicates that the molecular integrity of the tetramer itself remains unchanged during receptor binding and F triggering. Thus, efficient F triggering does not mandate complete separation of a tetrameric H stalk assembly, as proposed for an alternative H tetramer-SLAM cocrystal arrangement (form II in ref. 9). Rather, our study suggests that MeV H stalks form a single bundle, consistent with the recently described partial ectodomain structures of NDV (18) and PIV5 (19) HN proteins, and that F triggering does not mandate altering the overall integrity of this organization.

However, efficient F triggering requires structural flexibility between individual H monomers in the central section of the stalk bundle. Cysteine substitutions in this region (residues 110–114) completely abolish fusion-support activity, independent of whether the substitutions induce covalent tetramers or lead to an additional disulfide bond between monomers of an existing covalent H dimer. Considering our experience that unpaired stalk thiols result in intracellular retention of the protein, we assume that the engineered stalk cysteines are engaged in novel disulfide bonds. Confirmation for this notion comes from our observation that exposure of H-110C, H-111C, and H-112C complexes to reducing conditions partially restored fusion-support activity. This finding also demonstrates that the engineered disulfide bonds trap the H tetramer in a pre–F-triggering conformation. In contrast, disulfide bonds at position 114 inhibited fusion activation, even under reducing conditions. Because this variant also was fully intracellular transport competent, gross protein misfolding is unlikely. Alternatively, H-114C may assume a post–F-triggering–like conformation, or this substitution may impair interaction with F on a short-range basis.

Our successful previous engineering of N-linked glycans into consecutive positions (110-112) of the MeV H stalk highlights that each monomer enjoys a high degree of rotational freedom in this region (6). This flexibility is accentuated further by a modeling-predicted disturbance in the secondary structure of the monomers immediately upstream of residue 110. We postulate that local unraveling or rotational unwinding involving the central sections of each stalk monomer is required for F triggering (visualized schematically in Fig. 8*D*). Likewise, the stalk domains of the attachment proteins of many *Paramyxovirinae* subfamily members were implicated in F triggering (2, 16, 34). Our recent analysis of the related canine distemper virus H stalk domain (30) revealed a comparable requirement for structural freedom of the stalk center, suggesting a common theme of *Paramyxovirinae* attachment-protein–mediated fusion support.

The homodimer/heterotetramer complementation studies and native-PAGE assays prove that receptor binding induces biochemically appreciable conformational changes in the H tetramer. H homodimers harboring alanine substitutions in the central stalk section spontaneously assume an organization distinct from that of wild-type H dimers. They homotetramerize efficiently but are incapable of F binding (6) and are unable to associate into heterotetramers with standard H or any of the other complementation groups. However, exposure to physical stress, soluble receptor, or mAbs mimicking receptor binding through interaction with the RBS is sufficient to initiate the reorganization of standard H tetramers into an H-F111A-like conformation, suggesting that the latter may represent a final, postreceptor-binding/F-triggering structure. This hypothesis is substantiated by our demonstration that exposure to soluble receptor is sufficient to initiate F refolding in native, membrane-embedded paramyxovirus fusion complexes. The significance of this finding is threefold: It underscores the physiological significance of the H tetramer rearrangement observed in native-PAGE assays; it demonstrates that little external energy is required to trigger the *Paramyxovirinae* entry cascade; and it confirms that triggering is achieved readily at the plasma membrane under neutral pH conditions.

We note that, upon exposure to physical stress or soluble receptor, the F-triggering–defective H-I98A tetramers also undergo a conformational rearrangement resembling that of standard H tetramers. Previous studies have revealed a substantially higher F coimmunoprecipitation efficiency with H-I98A than with unmodified H; this finding was interpreted as indicating a stronger physical interaction of H-I98A F glycoprotein oligomer pairs (16). Our results may reflect that receptor binding to H-I98A is insufficient to induce the H tetramer rearrangements because of a stabilizing effect of tightly bound F. Alternatively, the H-I98A substitution could impair the separation of the two envelope glycoprotein complexes even after a receptor-induced H-I98A reorganization has occurred. Either scenario is compatible with our observation that exposure of H-I98A F complexes to membrane-integral or soluble receptor does not lead to the initiation of biochemically appreciable F-trimer refolding.

Because H-F111A could complement H-I98A or H-ΔCD46 functionally on a heterodimer level in previous complementation studies (8), we furthermore conclude that the H-F111A reorganization is not structurally dominant. For the related Nipah virus G attachment protein, rearrangements have been proposed based on exposure of an mAb epitope after receptor docking (35) and altered mAb reactivity after stalk mutagenesis (34). Because crystals of free and receptor-complexed G head domains show few structural differences (36), changes in the G oligomer organization likewise may lead to Nipah F triggering, suggesting that basic principles of fusion initiation indeed may be conserved across different *Paramyxovirinae* genera.

Last, additional conditions located downstream of receptor binding and the initial F triggering must be fulfilled for productive MeV F refolding and fusion pore formation. Conceivably, these requirements could comprise a demand for a defined proximity of donor and target membrane provided by the continued interaction of H with membrane-embedded receptor, the coordinated local assembly of multiple activated H/F complexes through receptor clustering in the target membrane, a requirement for additional physical force originating from H/receptor-driven local curvature in opposing donor and target membranes (37, 38), or, potentially a second contact between attachment and refolding F protein complexes (39) that is required to complete membrane merger but is not induced through the interaction of H with soluble receptor.

In conclusion, we postulate that the functional MeV membrane fusion machinery is comprised of preassembled H-F heterooligomers in a prereceptor-bound/F-triggering H tetramer and prefusion F trimer conformation (Fig. 8*D*). Upon ligand binding to at least one of the covalent dimer pairs in the H dimer-of-dimers, partial unwinding/unraveling of the central section of the H stalk domain ensues, most likely disrupting preexisting contacts between the stalk and the F trimer. Little energy is required for this

step, because docking of soluble receptor moieties initiates the process efficiently. The resulting change in microenvironment at the former H–F contact zone may be sufficient for F refolding to commence. Unwinding of the stalk center most likely coincides with a rearrangement of the H head domain dimer–dimer interface. However, the overall physical integrity of the H tetramer and the tetrameric arrangement of the upper section of the H stalk remain intact during the process.

Methods

Cell Lines, Viral Stocks and Transfections. Vero (African green monkey kidney epithelial) cells (CCL-81; ATCC) and Vero cells stably expressing human SLAM [Vero-SLAM cells (40)] were maintained in DMEM supplemented with 7.5% (vol/vol) FBS at 37 °C and 5% CO_2. At every third passage, Vero-SLAM cells were kept under G418 selection. Lipofectamine 2000 (Invitrogen) was used for all transient transfection reactions. Modified vaccinia virus Ankara expressing T7 polymerase (41) was amplified in DF-1 (chicken embryo fibroblast) cells (CRL-12203; ATCC).

Site-Directed Mutagenesis and Epitope Tagging. Site-directed mutagenesis was performed following the QuikChange protocol (Stratagene) using pCG_sH (42) as template. In addition, mutant constructs were epitope tagged, resulting in a set of H variants that contained either an N-terminal HA tag or a triple FLAG tag (43). A single or double copy of a single-chain antibody directed against the carcinoembryonic antigen (CEA) (25) was added to the H C terminus in some experiments to impart a significant change in molecular weight of the protein. Changes were confirmed by DNA sequencing in all cases.

Flow Cytometry for Analysis of H Expression and Receptor-Binding Capacity. Surface-expression levels of MeV H and the ability of MeV H variants to bind the SLAM receptor were monitored in a flow cytometer assay as previously described (6).

Quantitative Cell-to-Cell Fusion Assays. Cell-to-cell fusion was assessed using an established luciferase reporter assay as previously described (6, 8). For qualitative assessment, transfected Vero cells were photographed at the indicated times following transfection at a magnification of 200×. To quantify the extent of cell-to-cell fusion after partial reduction of engineered H disulfide bonds through DTT treatment, the number of nuclei present in discrete cells and in syncytia was quantified in multiple, randomly selected fields of view (magnification: 200×). The number of nuclei present in syncytia was determined by the difference in the number of individual cells counted in the negative control (F-only population) and the treated samples.

Statistical Analysis. To assess the statistical significance of differences between sample means, unpaired two-tailed *t* tests were applied using the Prism 5 (GraphPad) software package.

Envelope Glycoprotein Heterodimer Coimmunoprecipitation. Vero cells were transfected with equal amounts of the differently tagged H variants as indicated. Thirty-six hours posttransfection, cell-surface proteins were biotinylated with 0.5 mg/mL sulfosuccinimidyl-2-(biotinamido)ethyl-1,3-dithiopropionate (Thermo Scientific) for 20 min at 4 °C as previously described (6). Cleared supernatants were incubated with M2 mAb directed against the FLAG epitope (Sigma) at 4 °C. After precipitation with immobilized protein G at 4 °C, samples were washed and eluted in PBS, 2% SDS. The eluted material was diluted to 0.15% SDS with PBS, followed by adsorption of biotinylated protein material to immobilized streptavidin for 120 min at 4 °C. Bound material was eluted and denatured with urea buffer [200 mM Tris (pH 6.8), 8 M urea, 5% (wt/vol) SDS, 0.1 mM EDTA, 0.03% bromophenol blue, 1.5% (wt/vol) DTT] for 30 min at 50 °C, fractionated by SDS/PAGE, and blotted to PVD membranes. Immunoblots were decorated with α-FLAG (M2) and αHA (16b12) monoclonal antibodies, respectively, and were developed using an anti-mouse IgG light-chain conjugate and ChemiDoc XRS digital imaging system (Bio-Rad).

Detection of Envelope Glycoprotein Dimers on Cell Surface. Vero cells were transfected with 4 μg per well of MeV H-encoding DNA total, 2 μg of a FLAG-tagged H variant, and 2 μg of FLAG-tagged H variants containing a single-chain antibody moiety (XL) as indicated. Thirty-six hours posttransfection, cell-surface proteins were biotinylated with 0.5 mg/mL sulfosuccinimidyl-2-(biotinamido)ethyl-1,3-dithiopropionate as detailed above. Precipitates were washed as outlined above, split into two equal fractions, and denatured in urea buffer under reducing [urea buffer containing 1.5% (wt/vol) DTT] or nonreducing (urea buffer without DTT) conditions. Reduced samples were fractionated on 10% (wt/vol) SDS-Tris/glycine gels. Nonreduced samples were analyzed on 3–8% (wt/vol) NuPAGE Tris/Acetate gradient gels (Invitrogen).

Attachment Protein Homodimer Heterotetramer Gel-Shift Analysis. Vero cells were transfected with a total of 4 μg per well of MeV H-encoding DNA [1 μg encoding FLAG-tagged H variants and 3 μg encoding FLAG-tagged H featuring, in addition, a tandem copy of a single-chain α-CEA antibody (2XL)]. Thirty-six hours posttransfection, cells were subjected to native-PAGE analysis. Blots were visualized with α-FLAG M2 antibodies as described.

Cysteine Engineering and Assessment of Covalent H Tetramer Formation. Vero cells were transfected with 4 μg per well of MeV H-encoding plasmid DNA harboring individual cysteine substitutions as specified. Thirty-six hours posttransfection, cell-surface–exposed proteins were biotinylated as described. After precipitation with immobilized streptavidin, bound material was divided into two equal fractions, denatured under reducing (urea-DTT) or nonreducing (urea without DTT) conditions, and fractionated on 10% (wt/vol) SDS-Tris/glycine or 3–8% (wt/vol) NuPAGE Tris-Acetate gradient gels (Invitrogen). For densitometric analysis of immunoblots, signal intensities were quantified using the QuantityOne software package (Bio-Rad). The extent of covalent H tetramer formation was quantified by calculating for each individual mutant the ratio of H tetramer to total H material.

Native-PAGE and Native Gel Shift. Vero cells were transfected with 4 μg per well of plasmid DNA encoding different H constructs as specified. Thirty-six hours posttransfection, cells were washed with PBS, and protein was extracted using Native Tris Sample buffer [100 mM Tris·Cl, 10% glycerol, 0.0025% Bromophenol Blue (pH 8.6) with 0.1% digitonin] at 4 °C for 30 min. Samples were cleared (20,000 × *g* for 20 min) and fractionated on native-PAGE 3–12% (wt/vol) Bis-Tris gradient gels. PVDF blots were fixed with an 8% acetic acid wash for 10 min, followed by immunostaining and developing as outlined above.

For gel-shift experiments, antibodies (as specified) or affinity-purified soluble mouse Fc-SLAM receptor [sSLAM at 0.05 mg/mL final concentration (6)] were bound to H-protein–expressing cells on ice for 30 min before washing and digitonin extraction of proteins. In ex vivo binding experiments, digitonin extracts of H variants were prepared first and then were mixed with antibodies or sSLAM and incubated on ice for 30 min. In both cases, extracts were processed and subjected to native PAGE analysis as before.

Coimmunoprecipitation. To assess physical association of MeV H and F proteins, coimmunoprecipitation was carried out as previously described (6, 8).

In Situ Assessment of F Triggering. Vero cells were cotransfected with H-ΔCD46– and F-encoding plasmids, followed by incubation in the presence of fusion inhibitory peptide (FIP) as indicated to prevent any premature breakdown of the cell monolayer. Thirty-six hours posttransfection, cells were washed extensively to remove FIP and were subjected to surface immunoprecipitations by incubating intact monolayers in the presence of mAb [α-Flag M2 (Sigma) for control, α-pretrigger F(32), or α-triggered F(31); 1:750-dilution in DMEM each] at 4 °C to block conformational rearrangements of membrane-integral envelope glycoprotein complexes) or 37 °C to enable fusion for 1 h. Where specified, wells also received sSLAM or unspecific murine IgG (Sigma) at 0.05 mg/mL final concentration. Reference wells were overlaid with SLAM-positive Vero-SLAM cells before incubation at 37 °C. Subsequently, samples were incubated further for 1 h at 4 °C. Unbound antibody then was removed through extensive washing, cells were lysed in RIPA buffer, and cleared lysates were subjected to precipitation of immunocomplexes with immobilized protein G Sepharose and SDS/PAGE analysis as described above.

Dual Split-Protein Cell-Content–Mixing Assay. Vero cells were transfected with plasmids encoding H-ΔCD46, F, and dual-split protein (DSP_{1-7}) (33). In controls, H-encoding plasmid was omitted. A second population of Vero or Vero-SLAM cells was transfected with plasmids encoding SLAM and DSP_{8-11} (33) or DSP_{8-11} alone. As a reference for reconstitution of N-terminal (DSP_{1-7}) and C-terminal (DSP_{8-11}) GFP/renilla luciferase halves, controls were cotransfected with both DSP_{1-7} and DSP_{8-11} plasmids. Twenty-four hours posttransfection, cells were mixed at an equal ratio in the specified combinations and reseeded in black-walled 96-well plates; specified wells received sSLAM at 0.05 mg/mL final concentration. Cell-content mixing indicating fusion pore formation was monitored over a 12-h time window at 37 °C by following $DSP_{1-7\ and}\ DSP_{8-11}$ reconstitution resulting in restored renilla luciferase activity. As substrate, EnduRen (Promega) was added according to the manufacturer's

instruction. Plates were examined at 90-min intervals in a BioTek Synergy H1 plate reader in luminescence top-count area scan mode. For each replicate, relative luciferase units were calculated through normalization of individual measurements for the maximum readout found in the DSP_{1-7}/DSP_{8-11} double-transfected reference cell population. In some experiments, cell populations were reseeded into 12-well plates and incubated in the presence or absence of additional sSLAM (0.05 mg/mL final concentration), and fusion was assessed microscopically.

ACKNOWLEDGMENTS. We thank B. Horvat and M. Ehnlund for providing mAbs directed against the MeV F protein and G. Melikyan, N. Kondo, and Z. Matsuda for providing split-luciferase reporter plasmids. This work was supported, in part, by National Research Service Award/National Institute of Allergy and Infectious Disease (NIAID) F32 AI085763 from the National Institutes of Health (NIH)/NIAID (to M.A.B.) and by Public Health Service Grant AI083402 from the NIH/NIAID (to R.K.P.).

1. Lamb RA, Jardetzky TS (2007) Structural basis of viral invasion: Lessons from paramyxovirus F. *Curr Opin Struct Biol* 17:427–436.
2. Deng R, Mirza AM, Mahon PJ, Iorio RM (1997) Functional chimeric HN glycoproteins derived from Newcastle disease virus and human parainfluenza virus-3. *Arch Virol Suppl* 13:115–130.
3. Deng R, Wang Z, Mirza AM, Iorio RM (1995) Localization of a domain on the paramyxovirus attachment protein required for the promotion of cellular fusion by its homologous fusion protein spike. *Virology* 209:457–469.
4. Melanson VR, Iorio RM (2006) Addition of N-glycans in the stalk of the Newcastle disease virus HN protein blocks its interaction with the F protein and prevents fusion. *J Virol* 80:623–633.
5. Tanabayashi K, Compans RW (1996) Functional interaction of paramyxovirus glycoproteins: Identification of a domain in Sendai virus HN which promotes cell fusion. *J Virol* 70:6112–6118.
6. Paal T, et al. (2009) Probing the spatial organization of measles virus fusion complexes. *J Virol* 83:10480–10493.
7. Lee JK, et al. (2008) Functional interaction between paramyxovirus fusion and attachment proteins. *J Biol Chem* 283:16561–16572.
8. Brindley MA, Plemper RK (2010) Blue native PAGE and biomolecular complementation reveal a tetrameric or higher-order oligomer organization of the physiological measles virus attachment protein H. *J Virol* 84:12174–12184.
9. Hashiguchi T, et al. (2011) Structure of the measles virus hemagglutinin bound to its cellular receptor SLAM. *Nat Struct Mol Biol* 18:135–141.
10. Colf LA, Juo ZS, Garcia KC (2007) Structure of the measles virus hemagglutinin. *Nat Struct Mol Biol* 14:1227–1228.
11. Santiago C, Celma ML, Stehle T, Casasnovas JM (2010) Structure of the measles virus hemagglutinin bound to the CD46 receptor. *Nat Struct Mol Biol* 17:124–129.
12. Hashiguchi T, et al. (2007) Crystal structure of measles virus hemagglutinin provides insight into effective vaccines. *Proc Natl Acad Sci USA* 104:19535–19540.
13. Noyce RS, et al. (2011) Tumor cell marker PVRL4 (nectin 4) is an epithelial cell receptor for measles virus. *PLoS Pathog* 7:e1002240.
14. Hashiguchi T, Maenaka K, Yanagi Y (2011) Measles virus hemagglutinin: Structural insights into cell entry and measles vaccine. *Front Microbiol* 2:247.
15. Plemper RK, Hammond AL, Cattaneo R (2001) Measles virus envelope glycoproteins hetero-oligomerize in the endoplasmic reticulum. *J Biol Chem* 276:44239–44246.
16. Corey EA, Iorio RM (2007) Mutations in the stalk of the measles virus hemagglutinin protein decrease fusion but do not interfere with virus-specific interaction with the homologous fusion protein. *J Virol* 81:9900–9910.
17. Plemper RK, Brindley MA, Iorio RM (2011) Structural and mechanistic studies of measles virus illuminate paramyxovirus entry. *PLoS Pathog* 7:e1002058.
18. Yuan P, et al. (2011) Structure of the Newcastle disease virus hemagglutinin-neuraminidase (HN) ectodomain reveals a four-helix bundle stalk. *Proc Natl Acad Sci USA* 108:14920–14925.
19. Bose S, et al. (2011) Structure and mutagenesis of the parainfluenza virus 5 hemagglutinin-neuraminidase stalk domain reveals a four-helix bundle and the role of the stalk in fusion promotion. *J Virol* 85:12855–12866.
20. Yuan P, et al. (2005) Structural studies of the parainfluenza virus 5 hemagglutinin-neuraminidase tetramer in complex with its receptor, sialyllactose. *Structure* 13: 803–815.
21. Plemper RK, Hammond AL, Cattaneo R (2000) Characterization of a region of the measles virus hemagglutinin sufficient for its dimerization. *J Virol* 74:6485–6493.
22. Feige MJ, Hendershot LM (2011) Disulfide bonds in ER protein folding and homeostasis. *Curr Opin Cell Biol* 23:167–175.
23. Patterson JB, Scheiflinger F, Manchester M, Yilma T, Oldstone MB (1999) Structural and functional studies of the measles virus hemagglutinin: Identification of a novel site required for CD46 interaction. *Virology* 256:142–151.
24. Corey EA, Iorio RM (2009) Measles virus attachment proteins with impaired ability to bind CD46 interact more efficiently with the homologous fusion protein. *Virology* 383:1–5.
25. Hammond AL, et al. (2001) Single-chain antibody displayed on a recombinant measles virus confers entry through the tumor-associated carcinoembryonic antigen. *J Virol* 75:2087–2096.
26. Reisinger V, Eichacker LA (2008) Solubilization of membrane protein complexes for blue native PAGE. *J Proteomics* 71:277–283.
27. Corbin JD, et al. (2011) Metal ion stimulators of PDE5 cause similar conformational changes in the enzyme as does cGMP or sildenafil. *Cell Signal* 23:778–784.
28. Zettler J, Mootz HD (2010) Biochemical evidence for conformational changes in the cross-talk between adenylation and peptidyl-carrier protein domains of nonribosomal peptide synthetases. *FEBS J* 277:1159–1171.
29. Connolly SA, Leser GP, Yin HS, Jardetzky TS, Lamb RA (2006) Refolding of a paramyxovirus F protein from prefusion to postfusion conformations observed by liposome binding and electron microscopy. *Proc Natl Acad Sci USA* 103:17903–17908.
30. Ader N, et al. (2012) Structural rearrangements of the central region of the morbillivirus attachment protein stalk domain trigger F protein refolding for membrane fusion. *J Biol Chem* 287:16324–16334.
31. Malvoisin E, Wild F (1990) Contribution of measles virus fusion protein in protective immunity: Anti-F monoclonal antibodies neutralize virus infectivity and protect mice against challenge. *J Virol* 64:5160–5162.
32. Sheshberadaran H, Chen SN, Norrby E (1983) Monoclonal antibodies against five structural components of measles virus. I. Characterization of antigenic determinants on nine strains of measles virus. *Virology* 128:341–353.
33. Kondo N, Miyauchi K, Matsuda Z (2011) Monitoring viral-mediated membrane fusion using fluorescent reporter methods. *Curr Protoc Cell Biol*, Chapter 26:26.9.1–26.9.9.
34. Bishop KA, et al. (2008) Residues in the stalk domain of the hendra virus g glycoprotein modulate conformational changes associated with receptor binding. *J Virol* 82:11398–11409.
35. Aguilar HC, et al. (2009) A novel receptor-induced activation site in the Nipah virus attachment glycoprotein (G) involved in triggering the fusion glycoprotein (F). *J Biol Chem* 284:1628–1635.
36. Xu K, et al. (2008) Host cell recognition by the henipaviruses: Crystal structures of the Nipah G attachment glycoprotein and its complex with ephrin-B3. *Proc Natl Acad Sci USA* 105:9953–9958.
37. Plemper RK (2011) Cell entry of enveloped viruses. *Curr Opin Virol* 1:92–100.
38. Melikyan GB (2011) Membrane fusion mediated by human immunodeficiency virus envelope glycoprotein. *Curr Top Membr* 68:81–106.
39. Porotto M, et al. (2011) Spring-loaded model revisited: Paramyxovirus fusion requires engagement of a receptor binding protein beyond initial triggering of the fusion protein. *J Virol* 85:12867–12880.
40. Ono N, et al. (2001) Measles viruses on throat swabs from measles patients use signaling lymphocytic activation molecule (CDw150) but not CD46 as a cellular receptor. *J Virol* 75:4399–4401.
41. Sutter G, Ohlmann M, Erfle V (1995) Non-replicating vaccinia vector efficiently expresses bacteriophage T7 RNA polymerase. *FEBS Lett* 371:9–12.
42. Cathomen T, Naim HY, Cattaneo R (1998) Measles viruses with altered envelope protein cytoplasmic tails gain cell fusion competence. *J Virol* 72:1224–1234.
43. Zhang L, Hernan R, Brizzard B (2001) Multiple tandem epitope tagging for enhanced detection of protein expressed in mammalian cells. *Mol Biotechnol* 19:313–321.

Virology 435 (2013) 485–492

Contents lists available at SciVerse ScienceDirect

Virology

journal homepage: www.elsevier.com/locate/yviro

Canine distemper virus with the intact C protein has the potential to replicate in human epithelial cells by using human nectin4 as a receptor

Noriyuki Otsuki [a,*], Tsuyoshi Sekizuka [b], Fumio Seki [a], Kouji Sakai [a], Toru Kubota [a], Yuichiro Nakatsu [a], Surui Chen [c], Hideo Fukuhara [c], Katsumi Maenaka [c], Ryoji Yamaguchi [d], Makoto Kuroda [b], Makoto Takeda [a]

[a] Department of Virology 3, National Institute of Infectious Diseases, Gakuen 4-7-1, Musashimurayama, Tokyo 208-0011, Japan
[b] Laboratory of Bacterial Genomics, Pathogen Genomics Center, National Institute of Infectious Diseases, Tokyo, Japan
[c] Laboratory of Biomolecular Science, Faculty of Pharmaceutical Sciences, Hokkaido University, Sapporo, Japan
[d] Department of Veterinary Pathology, Faculty of Agriculture, University of Miyazaki, Miyazaki, Japan

ARTICLE INFO

Article history:
Received 12 August 2012
Returned to author for revisions
11 September 2012
Accepted 26 October 2012
Available online 19 November 2012

Keywords:
Canine distemper virus
Nectin4
Receptor
Morbillivirus

ABSTRACT

Recent outbreaks in monkeys have proven that canine distemper virus (CDV) causes diseases in a wide range of mammals. CDV uses SLAM and nectin4 as receptors to replicate in susceptible animals. Here, we show that human nectin4, but not human SLAM, is fully functional as a CDV receptor. The CDV Ac96I strain hardly replicated in nectin4-expressing human epithelial NCI-H358 cells, but readily adapted to grow in them. Unsurprisingly, no amino acid change in the H protein was required for the adaptation. The original Ac96I strain possessed a truncated C protein, and a subpopulation possessing the intact C protein was selected after growth in NCI-H358 cells. Other CDV strains possessing the intact C protein showed significantly higher growth abilities in NCI-H358 cells than the Ac96I strain with the truncated C protein. These findings suggest that the C protein is functional in human epithelial cells and critical for CDV replication in them.

Introduction

Distemper is an acute systemic infectious disease that mainly affects dogs and other canidae, and is caused by canine distemper virus (CDV) (Sawatsky et al., 2011). The disease is characterized by fever, coughing, vomiting, diarrhea, and neurological manifestations. CDV belongs to the genus *Morbillivirus* in the family *Paramyxoviridae*. Measles virus (MV), rinderpest virus, phocine distemper virus, Peste-des-petits-ruminants virus, and cetacean morbillivirus also belong to the genus, and cause severe acute systemic infections in humans, cows, seals, goats, and dolphins, respectively (Wang et al., 2012). The host range of these viruses is generally restricted to specific animal species. Recently, however, animals of many species, *Ailuridae* (Kotani et al., 1989), *Mustelidae* (Perpinan et al., 2008), *Viverridae* (Hirama et al., 2004; Hur et al., 1999), *Procyonidae* (Roscoe, 1993), *Phocidae* (Osterhaus et al., 1988), and *Felidae* (Appel et al., 1994; Roelke-Parker et al., 1996), have been naturally infected with CDV. Importantly, in the last several years, CDV has caused lethal outbreaks in nonhuman primates (Qiu et al., 2011; Sun et al., 2010).

Viruses in the genus *Morbillivirus* are enveloped viruses that possess a nonsegmented negative-stranded RNA genome encoding six genes, N, P/V/C, M, F, H, and L (Wang et al., 2012). The genome is encapsidated by the nucleocapsid (N) protein, forming a helical ribonucleocapsid that is associated with a viral RNA-dependent RNA polymerase composed of the phospho- (P) and large (L) proteins. In addition to the P protein, the P gene encodes two nonstructural proteins, V and C, by a process of RNA editing and an alternative translation initiation in a different reading frame, respectively (Wang et al., 2012). The V and C proteins are non-essential products, but play important roles in counteracting the host innate immune responses (Nakatsu et al., 2008; Rothlisberger et al., 2010; von Messling et al., 2006). On the envelope, there are two types of spike proteins, the hemagglutinin (H) and fusion (F) proteins. The H protein is responsible for receptor binding, while the F protein mediates membrane fusion between the viral envelope and the host cell plasma membrane. Both CDV and MV have been shown to use signaling lymphocyte activation molecule (SLAM) and nectin4 as receptors (Muhlebach et al., 2011; Noyce et al., 2011; Pratakpiriya et al., 2012; Seki et al., 2003; Tatsuo et al., 2000). SLAM is expressed on a subset of immune cells, while nectin4 is expressed at adherens junctions in the epithelial tissues of various organs (Takeda et al., 2011). Some neural cells in the central nervous system of dogs also

* Corresponding author. Fax: +81 42 562 8941.
E-mail address: otsuki@nih.go.jp (N. Otsuki).

0042-6822/$ - see front matter © 2012 Elsevier Inc. All rights reserved.
http://dx.doi.org/10.1016/j.virol.2012.10.033

express nectin4 and have been shown to be infected with CDV (Pratakpiriya et al., 2012). Although morbilliviruses commonly use SLAM as a receptor, each morbillivirus preferentially uses the SLAM of its host animals (Seki et al., 2003; Tatsuo et al., 2001). Tatsuo et al. (Tatsuo et al., 2001) reported that the HA7 strain of CDV isolated using B95a cells, which express marmoset SLAM, used human SLAM reasonably well, whereas the Onderstepoort CDV vaccine strain failed to use it. In the present study, we analyzed the ability of wild-type CDV strains to use human nectin4 and human SLAM as receptors. In addition, the genetic changes in CDV required for efficient growth in human epithelial cells were investigated.

Results and discussion

Ability of wild-type CDV strains to use human nectin4 and human SLAM as receptors

Our recent study showed that wild-type CDV strains use dog nectin4 as a receptor (Pratakpiriya et al., 2012). A human nectin4 cDNA was obtained from human lung carcinoma-derived NCI-H358 cells (Takeda et al., 2007), and Vero cells constitutively expressing human nectin4 (Vero/hNectin4) were generated using this cDNA. Flow cytometry analyses confirmed that Vero/hNectin4 cells expressed human nectin4, but the expression level was several-fold lower than that of dog nectin4 in Vero/dNectin4 cells (Pratakpiriya et al., 2012) (Fig. 1A). The MV H protein binds to the V domain of human nectin4 (Muhlebach et al., 2011; Noyce et al., 2011). We found six amino acid differences in the V domain between human nectin4 and dog nectin4 (DDBJ/Gen Bank accession numbers AB755430 and AB755429, respectively) (Fig. 2). The parental Vero, nectin4-expressing (Vero/dNectin4 (Pratakpiriya et al., 2012) and Vero/hNectin4) and SLAM-expressing (Vero/hSLAM (Ono et al., 2001) and Vero. DogSLAM tag (Seki et al., 2003)) Vero cells were infected with wild-type CDV strains (Ac96I, 82Con, 55L, M24Cr, and Th12). As reported previously (Pratakpiriya et al., 2012; Seki et al., 2003), no syncytia developed in the parental Vero cells infected with these CDV strains (Fig. 1B), although they may have had low levels of infection without causing syncytium formation, as shown for MV (Hashimoto et al., 2002). On the other hand, all the strains produced large syncytia in Vero/hNectin4 cells as efficiently as in Vero/dNectin4 cells (Fig. 1B). Syncytium formation was barely detectable in Vero/hSLAM cells, but clearly evident in Vero.DogSLAM tag cells (Fig. 1B). Thus, human SLAM seemed to be suboptimal as a wild-type CDV receptor. The growth kinetics of Ac96I in the parental Vero, Vero/dNectin4, and Vero/hNectin4 cells were analyzed. Ac96I did not replicate in Vero cells, but showed efficient replication in both Vero/dNectin4 and Vero/hNectin4 cells (Fig. 1C). The replication kinetics in Vero/dNectin4 and Vero/hNectin4 cells were comparable with one another (Fig. 1C). To show the direct contribution of the H protein to the syncytium formation, cell-to-cell fusion assays were performed using mammalian cell expression vectors. In all of the cell lines, no syncytia were observed when the F protein was expressed alone (Fig. 3). When the H protein of Ac96I was expressed together with the F protein, large syncytia developed in Vero/hNectin4 and Vero/dNectin4 cells, but not in the parental Vero cells (Fig. 3). The susceptibilities of Vero, Vero/dNectin4, and Vero/hNectin4 cells to Ac96I infection were analyzed and compared. The infectivity of Ac96I in Vero/hNectin4 cells determined by the 50% cell culture infectious dose ($CCID_{50}$) was 4.25 ± 0.00 $CCID_{50}$/ml, which was comparable to that in Vero/dNectin4 cells (4.58 ± 0.12 $CCID_{50}$/ml). The titer determined in Vero cells was less than 1.75 $CCID_{50}$/ml. These data demonstrate that human nectin4 functions as a CDV receptor as efficiently as dog nectin4, while human SLAM does not.

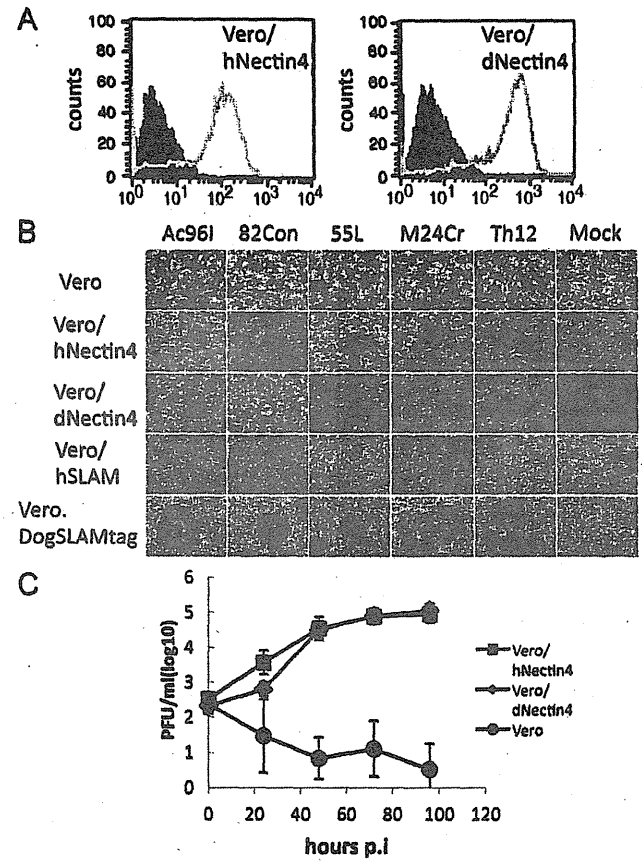

Fig. 1. Infection of the parental, nectin4-expressing, and SLAM-expressing Vero cells with wild-type CDV strains. (A) Vero/hNectin4 (left panel) and Vero/dNectin4 (right panel) cells were stained with a goat anti-human nectin4 polyclonal antibody (gray empty profile) or a control goat IgG (filled black profile), followed by staining with Alexa Fluor 488-conjugated anti-goat IgG. (B) Vero, Vero/hNectin4, Vero/dNectin4, Vero/hSLAM, and Vero.DogSLAMtag cells were infected with wild-type CDV strains (Ac96I-VDS, 82Con, 55L, M24Cr, and Th12) or mock-infected. At 48 h (Vero, Vero/hNectin4, Vero/dNectin4, and Vero/hSLAM) or 24 h (Vero.DogSLAMtag) post-infection, the cells were stained with the Giemsa solution, and observed under a phase-contrast microscope. (C) Replication kinetics of Ac96I. Vero/hNectin4, Vero/dNectin4, and parental Vero cells were infected with Ac96I at a MOI of 0.01. At various time intervals post-infection, the virus titers were determined by plaque assays.

The pathology of morbilliviruses is well documented for MV. MV is an airborne virus, and the infection starts via SLAM-mediated entry into alveolar macrophages and dendritic cells in the lung or respiratory tracts. After replicating in local lymph nodes, MV spreads to various lymphoid organs or tissues throughout the body using SLAM as a receptor (Takeda et al., 2011). Thus, the ability to use SLAM is critical for MV, and probably for all morbilliviruses, to spread and cause diseases in vivo. Conversely, nectin4 is used at the late stage of infection to shed progeny viruses into the respiratory tract (Takeda et al., 2011). Thus, the low capacity for using human SLAM would explain the inability of CDV to replicate in humans.

Potential of wild-type CDV strains to replicate in human epithelial cells

The host range of MV is determined by not only receptors but also intracellular factors (Iwasaki and Yanagi, 2011). NCI-H358 cells are highly susceptible and permissive to MV infection (Takeda et al., 2007). NCI-H358 cells were found to express human nectin4, although the expression level was significantly

```
human   32 GELETSDVVTVVLGQDAKLPCFYRGDSGEQVGQVAWARVDAGEGAQELALLHSKYGLHVS  91
dog     31 .......L.................P.................R.............  90
mouse   31 ........................PD...........PN..IR............N  90

human   92 PAYEGRVEQPPPPRNPLDGSVLLRNAVQADEGEYECRVSTFPAGSFQARLRLRVLV  147
dog     91 A............S....A.....................................  146
mouse   91 ....D.........D.................................M......  146
```

Fig. 2. Amino acid sequence comparison of the V domains of human, dog, and mouse nectin4. Dots indicate identical residues to those of human nectin4.

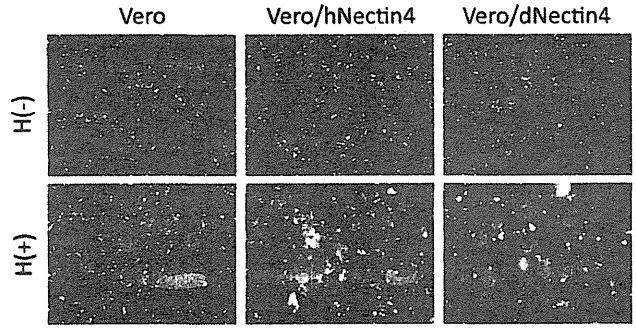

Fig. 3. Cell-to-cell fusion assays. Vero (left panels), Vero/hNectin4 (middle panels), and Vero/dNectin4 (right panels) cells were transfected with the mCherry-expressing plasmid and the F protein-expressing plasmid (upper panels) or the mCherry-expressing plasmid and both the F protein-expressing plasmid and H protein-expressing plasmid (bottom panels). At 48 h post-transfection, the cells were observed using an Axio Observer.D1 microscope.

lower than that in Vero/hNectin4 cells (Fig. 4A). Nevertheless, MV replicates in these cells in a nectin4-dependent manner (Muhlebach et al., 2011; Noyce et al., 2011). NCI-H358 cells were infected with wild-type CDV strains (Ac96I, 82Con, 55L, M24Cr, and Th12) at a multiplicity of infection (MOI) of 0.01, and the infectious virus titers were determined at 5 days post-infection (Fig. 4B). The data showed that the virus titer of the Ac96I strain was significantly lower than those of the other four wild-type CDV strains (Fig. 4B). The Ac96I strain was originally isolated from the large intestine of dogs with distemper using Vero.DogSLAMtag cells (Lan et al., 2006) and passaged 2–3 times in Vero.DogSLAMtag cells to obtain a sufficient amount of virus stocks for analysis. In the following experiments, the Vero.DogSLAMtag cell-grown Ac96I strain was designated Ac96I-VDS. NCI-H358 cells were infected with Ac96I-VDS, and the virus titers were determined at 1, 3, 5, and 7 days post-infection (Fig. 4C). The results confirmed that Ac96I-VDS replicated poorly in NCI-H358 cells (Fig. 4C). Nevertheless, at 7 days post-infection, some production of infectious viruses was observed in Ac96I-infected NCI-H358 cells (Fig. 4C). After eight passages of Ac96I-VDS in NCI-H358 cells, the CDV-infected cells were scraped into culture medium, subjected to three cycles of freezing-and-thawing, and centrifuged. The supernatants were collected. The NCI-H358 cell-grown CDV was designated Ac96I-H358. Fresh monolayers of NCI-H358 cells were infected with Ac96I-H358, and the replication kinetics were analyzed at various time intervals. The data showed that Ac96I-H358 replicated well in NCI-H358 cells and produced infectious virus particles efficiently (Fig. 4B). To confirm the growth ability of Ac96I-H358 in human epithelial cells, the replication kinetics of Ac96I-VDS and Ac96I-H358 were analyzed in another nectin4-positive human epithelial cell line, II-18 (Shirogane et al., 2010). Both Ac96I-VDS and Ac96I-H358 were able to replicate in II-18 cells (Fig. 4D). However, the replication ability of Ac96I-H358 was obviously greater than of Ac96I-VDS in II-18 cells, as observed in NCI-H358 cells (Fig. 4C and D). These findings confirmed that Ac96I-H358 exhibits restored ability to grow in human epithelial cells.

Genetic changes in the Ac96I-H358 strain during propagation in human epithelial NCI-H358 cells

Similar to other RNA viruses, CDV forms quasispecies. The nucleotide sequences of Ac96I-VDS and Ac96I-H358 were deeply analyzed by next-generation sequencing. Table 1 shows a list of the nucleotide substitutions acquired by Ac96I-H358, as well as selected preexisting nucleotides, during the eight passages of Ac96I-H358 in NCI-H358 cells. All of the nucleotide positions where more than 15% of the Ac96I-H358 genome acquired a nucleotide substitution or the proportion of preexisting nucleotides was increased by more than 15% are listed in Table 1. Unsurprisingly, these data showed no amino acid change in the H protein during the passages in NCI-H358 cells. These data strengthen the above conclusion that the CDV H protein possesses an intrinsic ability to use human nectin4 as a receptor. Our previous data for other wild-type strains also demonstrated that no amino acid changes occurred in the H protein during isolation from tissues of dogs with distemper and passages in Vero.DogSLAMtag cells (Lan et al., 2005a). Therefore, the ability to use human nectin4 is an intrinsic phenotype of wild-type CDV strains. The most striking change was observed in the P gene. The P gene encodes a polymerase cofactor protein, P, and two nonstructural proteins, C and V. Although the C and V proteins are nonessential for virus replication in cultured cells, they play crucial roles in counteracting the host innate immune responses (Devaux et al., 2007; Nakatsu et al., 2008; Rothlisberger et al., 2010; von Messling et al., 2006). The majority (91%) of Ac96I-VDS had a thymine at nucleotide position 2198, producing a truncated C protein, while the remaining 9% possessed the intact C protein (Table 1). The truncated C protein had a nonsense mutation at amino acid position 126 and became shorter by 49 amino acids, compared with the intact C protein (the site of the authentic stop codon was predicted by analyses of other wild-type CDV strains and previously reported CDV sequences (Fig. 5) (Wang et al., 2012)). The other four wild-type CDV strains (82Con, 55L, M24Cr, and Th12) possessed the intact C protein (Fig. 5). For MV, a truncation of the C protein at amino acid position 157 made the C protein defective in its ability to counteract the host interferon system (Nakatsu et al., 2008). The C protein sequence was perfectly (100%) restored in Ac96I-H358 (Table 1). These findings suggest that expression of the intact C protein was critical for replication in NCI-H358 cells, but not in Vero.DogSLAMtag cells. The nucleotide substitution in the P gene also caused a valine-to-alanine substitution at amino acid position 133 in the P protein (Table 1). P gene mutations accompanied by truncation or mutations in the C protein are often observed in the genome of Vero cell-grown MV strains (Miyajima et al., 2004; Takeda et al., 1998; Takeuchi et al., 2000). Vero cells are defective in the production of interferons (Chew et al., 2009; Emeny and Morgan, 1979), whereas NCI-H358 cells possess a functional interferon system (Ikegame et al., 2010). Thus, it is most likely that the truncation mutation for the C protein in Ac96I-VDS occurred in Vero.DogSLAMtag cells, rather than occurring in nature, since the C protein plays an important role for CDV pathogenesis in vivo (von Messling et al., 2006). Recently, Vero-based cell lines, e.g., Vero/hSLAM for MV,

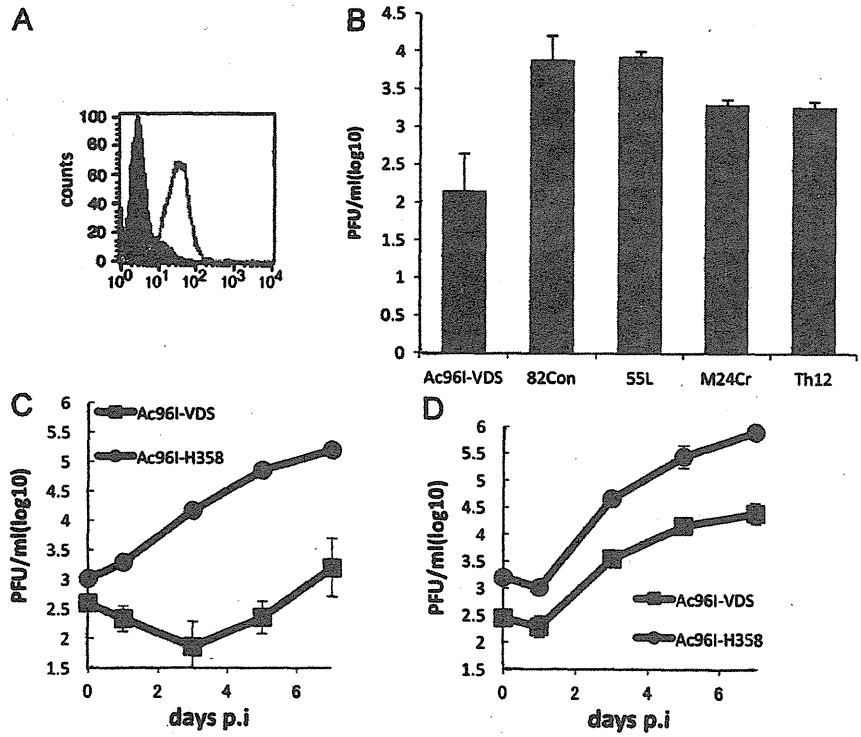

Fig. 4. Replication kinetics in NCI-H358 cells. (A) NCI-H358 cells were stained with a goat anti-human nectin4 polyclonal antibody (gray empty profile) or a control goat IgG (filled black profile), followed by staining with Alexa Fluor 488-conjugated anti-goat IgG. (B) NCI-H358 cells were infected with the Ac96I-VDS, 82Con, 55 L, M24Cr, or Th12 CDV strains at a MOI of 0.01. At 5 days post-infection, the virus titers were determined by plaque assays. (C, D) NCI-H358 (C) and II-18 (D) cells were infected with Ac96I-VDS or Ac96I-H358 at a MOI of 0.01. At 1, 3, 5, and 7 days post-infection, the virus titers were determined by plaque assays.

Table 1
Acquired and selected nucleotides during passages in NCI-H358 cells.

		Ac-96I-VDS					Ac-96I-H358						
			Proportion (%)					Proportion (%)					
Gene	Nucleotide position	Total no. of reads	A	C	G	T	Total no. of reads	A	C	G	T	Protein	Amino acid substitution
N	792	349	0	0	0	100	138	0	0	75[a]	25	N	L229V
N	974	541	0	1	0	99	148	0	32	0	68	n.a.[b]	no
N	995	340	0	0	0	100	116	0	0	43	57	N	I296M
N	1506	100	0	0	100	0	33	18	0	82	0	N	E467K
P/V/C	2198	1024	0	9	0	91	101	0	100	0	0	P and VC	V133A 126Q[c]
M	3681	364	98	0	2	0	73	78	22	0	0	M	T84P
M	3965	63	0	0	0	100	46	50	0	0	50	M	F178L
M	4047	48	100	0	0	0	37	73	0	27	0	M	N206D
M	4417	81	84	0	0	16	31	100	0	0	0	M	L329Q
F	5926	196	0	78	22	1	61	0	100	0	0	F	R331P
F	6074	167	26	0	74	0	37	97	0	3	0	n.a.	no
L	9107	194	2	0	98	0	23	17	0	82	0	n.a.	no
L	14271	39	72	0	28	0	50	100	0	0	0	L	D1748N

[a] Acquired and selected nucleotides are underlined.
[b] Not applicable.
[c] A termination codon at position 126 was replaced with a glutamine residue.

have been used for the isolation of many viruses. Indeed, the interferon-deficient phenotype of Vero cells is an advantage for virus isolation. However, it may lead to the selection of a minor clone with a low ability to counteract the host innate immune responses. In this regard, use of lymphocyte-based cell lines and epithelial cell lines with a functional interferon system is advisable for the isolation of viruses for pathogenesis studies. In either case, our data showed that the P gene in the 9% population of Ac96I-VDS, which became 100% dominant in Ac96I-H358 cells, encoded C and V proteins that were functional for counteracting the human interferon system.

Although the C protein appears to play a critical role for CDV replication in NCI-H358 cells, mutations in other genes or proteins may contribute to the Ac96I-H358 growth in these cells, since the virus titer of Ac96I-H358 at 5 days post-infection was ~10-fold greater than those of the other wild-type CDV strains possessing the intact C protein (Fig. 4B, C). The data obtained by next-generation sequencing also showed that certain proportions

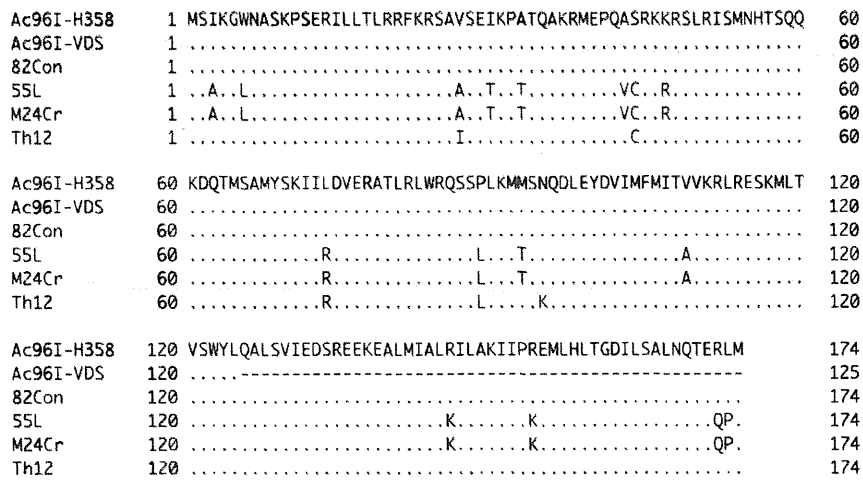

Fig. 5. Amino acid sequence comparison of the C protein. Dots indicate identical residues to the Ac96I-H358 strain. Bars indicate that there are no amino acid residues at these positions.

of Ac96I-H358 have nonsynonymous substitutions in the N and M genes (Table 1). These substitutions were leucine-to-valine, isoleucine-to-methionine, and glutamic acid-to-lysine at amino acid positions 129, 296, and 467 (L129V, I296M, and E467K), respectively, in the N protein, and threonine-to-proline, phenylalanine-to-leucine, and asparagine-to-aspartic acid at amino acid positions 84, 178, and 206 (T84P, F178L, and N206D), respectively, in the M protein (Table 1). Some mutations in the M protein of MV were shown to contribute to virus growth in unnatural host cells (Dong et al., 2009; Miyajima et al., 2004; Tahara et al., 2005, 2007). Therefore, it is of great interest to evaluate whether mutations in the M and N proteins are critical for CDV adaptation to be able to grow in human cells.

In addition, the M gene possessed a selected nonsynonymous substitution at position 4417 and both the F and L genes of Ac96I-H358 possessed a single selected nonsynonymous substitution (L329Q, R331P, and D1748N in the M, F, and L proteins, respectively) (Table 1). However, these mutations did not seem to be important for CDV to acquire the capacity to replicate well in NCI-H358 cells, since the major population (72–84%) of Ac96I-VDS already possessed these substitutions (Table 1). Since CDV possesses a nonsegmented RNA genome, some unnecessary mutations could be accompanied by significant changes, which exist on the same RNA genome.

Tatsuo et al. (2001) demonstrated that the CDV HA7 strain, but not the Onderstepoort CDV vaccine strain, used human SLAM reasonably well. However, our data showed that wild-type CDV strains used human SLAM poorly, similar to the case for the Onderstepoort vaccine strain. Since the HA7 strain was isolated using marmoset SLAM-expressing B95a cells, it may have adapted to use nonhuman primate SLAM as well as human SLAM. Thus, the Onderstepoort vaccine strain, rather than the HA7 strain, may have retained the original phenotype regarding the ability to use human SLAM. The data for the HA7 strain described in Tatsuo et al. (2001) may rather suggest that CDV easily adapts to the use of human SLAM. Seki et al. (2003) demonstrated that only a few amino acid changes in the H protein are sufficient for wild-type CDV strains to use marmoset SLAM efficiently, although they did not examine whether these changes conferred the ability to use human SLAM on the wild-type CDV strains. Unlike human SLAM, human nectin4 was fully functional as a wild-type CDV receptor. Despite this ability, Ac96I-VDS failed to spread in a human epithelial cell line. However, this phenotype is unlikely to be the original phenotype of wild-type CDV strains. Instead, they may have an intrinsic potential to replicate in human cells. In addition, the restoration of the C protein observed in the Ac96I-H358 strain implies that the CDV C protein is capable of counteracting human innate immune responses. Indeed, the CDV strains possessing the intact C protein showed reasonable degrees of ability to replicate in human epithelial cells. Nevertheless, the virus titers of these CDV strains in NCI-H358 cells were still lower than that of MV (data not shown) (Takeda et al., 2007). Some intracellular human host factors may not be optimal for the CDV replication machinery. Importantly, the Ac96I-H358 strain, which adapted to growth in NCI-H358 cells, showed a significantly higher replication potential than the other CDV strains in NCI-H358 cells, and its growth ability approached that of MV.

The critical factors that create the species barrier of CDV between susceptible animals and humans still remain unknown. However, some CDV strains appear to have already adapted to growth in nonhuman primates (Qiu et al., 2011; Sun et al., 2010). CDV is closely related to MV, and the major structural proteins of these viruses have some immunological cross-reactivity, such that immunity raised against MV proteins is partially, but insufficiently, effective against CDV infection (Giraudon and Wild, 1981; Norrby and Appel, 1980; Orvell and Norrby, 1980; Stephenson and ter Meulen, 1979; Taylor et al., 1991). Furthermore, some viral proteins of CDV and MV are even functionally exchangeable (Brown et al., 2005). The CDV genome forms an active ribonucleocapsid complex with the N, P, and L proteins of MV, and synthesizes viral RNAs using the MV proteins, and vice versa (Brown et al., 2005). Thus, immunity against MV may have protected humans against CDV infection. However, based on the present experimental data and the observation of large CDV outbreaks in monkeys (Qiu et al., 2011; Sun et al., 2010), we suggest that CDV has sufficient latent potential to adapt to humans, and may cause a serious disease in humans in the future. We thus propose that the preparation of a countermeasure against CDV needs to be seriously considered at the present time.

Materials and methods

Cells and viruses

Vero cells were maintained in DMEM supplemented with 5% fetal bovine serum (FBS). Vero.DogSLAMtag, Vero/hSLAM, and

Vero/dNectin4 cells were reported previously (Pratakpiriya et al., 2012; Seki et al., 2003) and maintained in DMEM supplemented with 5% FBS and 1 mg/ml geneticin (G418; Invitrogen Life Technologies, Carlsbad, CA). NCI-H358 cells (Takeda et al., 2007) and II-18 cells (Shirogane et al., 2010) were maintained in RPMI medium supplemented with 10% fetal calf serum. Total RNA obtained from NCI-H358 cells was used to synthesize the cDNA of human nectin4. The primers used for amplification of the human nectin4 cDNA were 5′-*GAATTC*AGTCTGCCTTTCAACCA-3′ and 5′-*GCGGCCGC*AGGCAGGCCTGGGTCA-3′ (sequences corresponding to EcoRI and NotI sites are shown in italics). The human nectin4 cDNA fragment was inserted into the pCXN2 vector, generating pCXN2-hNectin4. A Vero cell clone stably expressing human nectin4 (Vero/hNectin4) was generated by transfecting Vero cells with pCXN2-hNectin4. Vero/hNectin4 cells were maintained in DMEM supplemented with 5% FBS and 1 mg/ml geneticin. The wild-type Ac96I strain of CDV was isolated from the large intestine of dogs with distemper using Vero.DogSLAMtag cells (Lan et al., 2006), and the working stock of the Ac96I strain, which was passaged in Vero.DogSLAMtag cells 2–3 times in total, was designated Ac96I-VDS. The other wild-type CDV strains (82Con, 55L, M24Cr, and Th12) were isolated from morbid or dead dogs with distemper using Vero.DogSLAMtag cells, and reported previously (Lan et al., 2009; Lan et al., 2006; Lan et al., 2005b). To obtain an NCI-H358 cell-adapted Ac96I strain, Ac96I-VDS was inoculated into monolayers of NCI-H358 cells and passaged eight times in these cells. After the eight passages, the CDV-infected cells were scraped into culture medium, subjected to three cycles of freezing-and-thawing, and centrifuged. The supernatant was collected. The NCI-H358 cell-adapted Ac96I strain was designated Ac96I-H358.

Flow cytometry

The cell surface expression of nectin4 was analyzed using a goat anti-human nectin4 polyclonal antibody (R&D Systems, Minneapolis, MN) as the primary antibody and Alexa Fluor 488-conjugated anti-goat IgG (Molecular probes, Eugene, Oregon) as the secondary antibody. Normal goat IgG (PEPROTECH, Rocky Hill, NJ) was used as a control. The cell surface fluorescence of 1×10^4 cells was analyzed using a FACSCalibur flow cytometer (Becton Dickinson, Franklin Lakes, NJ).

Replication kinetics

Monolayers of Vero, Vero.DogSLAMtag, Vero/dNectin4, and NCI-H358 cells in 24-well plates were infected with Ac96I-VDS or Ac96I-H358 at a MOI of 0.01 per cell. After various time intervals, the cells were scraped into the culture supernatants, and the virus titers (PFU) were determined by plaque assays in Vero.DogSLAMtag cells.

Plaque titration

Monolayers of Vero.DogSLAMtag cells in 6-well cluster plates were infected with serially diluted virus samples, incubated for 1 h at 37 °C, and overlaid with 3 ml of minimal essential medium containing 2% FBS and 0.8% agarose (0.8% agarose-MEM). At 7 days post-infection, 2 ml of 0.8% agarose-MEM containing 0.01% neutral red was overlaid on each well, and the PFU was determined by counting the number of plaques at 2 days after the procedure.

Cell susceptibility to CDV infection

To analyze the susceptibility of Vero, Vero/dNectin4, and Vero/hNectin4 cells to Ac96I-VDS infection, serially diluted virus samples were inoculated into monolayers of these cells, and the $CCID_{50}$ of Ac96I-VDS in these cells was determined.

Cell-to-cell fusion assay

DNA fragments encoding the H protein of Ac96I-VDS and the CDV F protein were amplified and cloned into the pCAGGS vector. Vero, Vero/dNectin4, and Vero/hNectin4 cells were seeded in 12-well plates, and transfected with the F protein-expressing plasmid (0.3 μg) with or without the H protein-expressing plasmid (0.3 μg) using the TransIT-LT1 reagent (Mirus Bio, Madison, WI). To clearly detect syncytia, a fluorescent protein-expressing plasmid (pCA7-FR-mCherry; 0.3 μg) was included into the transfection mixture, as reported previously (Seki et al., 2011). At 48 h post-transfection, the cell monolayers were observed using an Axio Observer.D1 microscope.

Next-generation sequencing

Culture supernatants of Vero.DogSLAMtag and NCI-H358 cells infected with Ac96I-VDS and Ac96I-H358, respectively, were collected, and the virus particles were centrifuged into pellets through 30% sucrose cushions (30% sucrose [wt/vol] in NTE [0.1 M NaCl, 0.01 M Tris pH 7.4, 0.001 M EDTA]) at 185,000 × *g* for 2 h in a Beckman 45 Ti rotor at 4 °C. Subsequently, viral RNA was purified from the virus particles using Isogen (Nippon Gene, Tokyo, Japan). An RNAseq library was prepared using a ScriptSeq™ v2 RNA-Seq Library Preparation Kit (Illumina-compatible) (Epicentre Biotechnologies, Madison, WI) and the indexing method. Deep sequencing runs for pair-end short reads were performed with MiSeq and GAIIx systems (Illumina, San Diego, CA). To identify nucleotide variations based on the RNAseq analysis, the obtained short reads were mapped to the corresponding reference CDV genome sequence (Ac96I-VDS) by the BWA mapping tool (Li and Durbin, 2010). The obtained mapping data were visualized with GenomeJack viewer software (Mitsubishi Space Software, Tokyo, Japan).

Sequencing of the P gene of CDV strains

Viral RNAs were extracted from each virus stock using a High Pure Viral RNA Kit (Roche Diagnostics GmbH, Mannheim, Germany) according to the manufacturer's instructions. First-strand cDNA was synthesized using Super ScriptIII reverse transcriptase (Invitrogen, Carlsbad, CA), and then amplified by PCR using Prime STAR GXL DNA polymerase (Takara Bio, Shiga, Japan). The primers used for amplification and sequencing are available upon request. The PCR products were purified using a QIAquick Gel Extraction Kit (Qiagen KK, Tokyo, Japan). The nucleotide sequences of the purified PCR products were determined using a Big Dye Terminator v3.1 Cycle Sequencing Kit (Applied Biosystems, Foster City, CA) and a capillary sequencer.

Nucleotide sequence accession numbers

The short reads obtained by the next-generation sequencing have been deposited in the DDBJ Sequence Read Archive (DRA) of Japan (accession number: DRA000586). The consensus genome nucleotide sequences of Ac96I-VDS and Ac96I-H358 have been deposited in DDBJ/GenBank with accession numbers AB753775 and AB753776, respectively. The nucleotide sequences for the P gene of 55L, Th12, M24Cr, and 82Con have been deposited in

DDBJ/GenBank with accession numbers AB755425, AB755426, AB755427, and AB155428, respectively.

Acknowledgments

We thank Dr. Yusuke Yanagi for providing the Vero.DogSLAM-tag and Vero/hSLAM cells. We also thank all the members of Department of Virology 3, NIID, Japan, for technical support and valuable suggestions. This work was supported, in part, by grants from the Ministry of Education, Culture, Sports, Science and Technology and the Ministry of Health, Labour and Welfare of Japan, and a grant from The Takeda Science Foundation.

References

Appel, M.J., Yates, R.A., Foley, G.L., Bernstein, J.J., Santinelli, S., Spelman, L.H., Miller, L.D., Arp, L.H., Anderson, M., Barr, M., et al., 1994. Canine distemper epizootic in lions, tigers, and leopards in North America. J. Vet. Diagn. Invest.: Official Publication of the American Association of Veterinary Laboratory Diagnosticians, Inc. 6, 277–288.

Brown, D.D., Collins, F.M., Duprex, W.P., Baron, M.D., Barrett, T., Rima, B.K., 2005. 'Rescue' of mini-genomic constructs and viruses by combinations of morbillivirus N, P and L proteins. J. Gen. Virol. 86, 1077–1081.

Chew, T., Noyce, R., Collins, S.E., Hancock, M.H., Mossman, K.L., 2009. Characterization of the interferon regulatory factor 3-mediated antiviral response in a cell line deficient for IFN production. Molecular immunology 46, 393–399.

Devaux, P., von Messling, V., Songsungthong, W., Springfeld, C., Cattaneo, R., 2007. Tyrosine 110 in the measles virus phosphoprotein is required to block STAT1 phosphorylation. Virology 360, 72–83.

Dong, J.B., Saito, A., Mine, Y., Sakuraba, Y., Nibe, K., Goto, Y., Komase, K., Nakayama, T., Miyata, H., Iwata, H., Haga, T., 2009. Adaptation of wild-type measles virus to cotton rat lung cells: E89K mutation in matrix protein contributes to its fitness. Virus Genes 39, 330–334.

Emeny, J.M., Morgan, M.J., 1979. Regulation of the interferon system: evidence that Vero cells have a genetic defect in interferon production. J. Gen. Virol. 43, 247–252.

Giraudon, P., Wild, T.F., 1981. Differentiation of measles virus strains and a strain of canine distemper virus by monoclonal antibodies. J. Gen. Virol. 57, 179–183.

Hashimoto, K., Ono, N., Tatsuo, H., Minagawa, H., Takeda, M., Takeuchi, K., Yanagi, Y., 2002. SLAM (CD150)-independent measles virus entry as revealed by recombinant virus expressing green fluorescent protein. J. Virol. 76, 6743–6749.

Hirama, K., Goto, Y., Uema, M., Endo, Y., Miura, R., Kai, C., 2004. Phylogenetic analysis of the hemagglutinin (H) gene of canine distemper viruses isolated from wild masked palm civets (Paguma larvata). J. Vet. Med. Sci. /Jpn. Soc. Vet. Sci. 66, 1575–1578.

Hur, K., Bae, J.S., Choi, J.H., Kim, J.H., Kwon, S.W., Lee, K.W., Kim, D.Y., 1999. Canine distemper virus infection in binturongs (Arctictis binturong). J. Comp. Pathol. 121, 295–299.

Ikegame, S., Takeda, M., Ohno, S., Nakatsu, Y., Nakanishi, Y., Yanagi, Y., 2010. Both RIG-I and MDA5 RNA helicases contribute to the induction of alpha/beta interferon in measles virus-infected human cells. J. Virol. 84, 372–379.

Iwasaki, M., Yanagi, Y., 2011. Expression of the Sendai (murine parainfluenza) virus C protein alleviates restriction of measles virus growth in mouse cells. Proc. Nat. Acad. Sci. U.S.A. 108, 15384–15389.

Kotani, T., Jyo, M., Odagiri, Y., Sakakibara, Y., Horiuchi, T., 1989. Canine distemper virus infection in lesser pandas (Ailurus fulgens). Nihon juigaku zasshi. Jpn. J. Vet. Sci. 51, 1263–1266.

Lan, N.T., Yamaguchi, R., Furuya, Y., Inomata, A., Ngamkala, S., Naganobu, K., Kai, K., Mochizuki, M., Kobayashi, Y., Uchida, K., Tateyama, S., 2005a. Pathogenesis and phylogenetic analyses of canine distemper virus strain 007Lm, a new isolate in dogs. Vet. Microbiol. 110, 197–207.

Lan, N.T., Yamaguchi, R., Hirai, T., Kai, K., Morishita, K., 2009. Relationship between growth behavior in vero cells and the molecular characteristics of recent isolated classified in the Asia 1 and 2 groups of canine distemper virus. J. Vet. Med. Sci./Jpn. Soc. Vet. Sci. 71, 457–461.

Lan, N.T., Yamaguchi, R., Inomata, A., Furuya, Y., Uchida, K., Sugano, S., Tateyama, S., 2006. Comparative analyses of canine distemper viral isolates from clinical cases of canine distemper in vaccinated dogs. Vet. Microbiol. 115, 32–42.

Lan, N.T., Yamaguchi, R., Uchida, K., Sugano, S., Tateyama, S., 2005b. Growth profiles of recent canine distemper isolates on Vero cells expressing canine signaling lymphocyte activation molecule (SLAM). J. Comp. Pathol. 133, 77–81.

Li, H., Durbin, R., 2010. Fast and accurate long-read alignment with Burrows-Wheeler transform. Bioinformatics 26, 589–595.

Miyajima, N., Takeda, M., Tashiro, M., Hashimoto, K., Yanagi, Y., Nagata, K., Takeuchi, K., 2004. Cell tropism of wild-type measles virus is affected by amino acid substitutions in the P, V and M proteins, or by a truncation in the C protein. J. Gen. Virol. 85, 3001–3006.

Muhlebach, M.D., Mateo, M., Sinn, P.L., Prufer, S., Uhlig, K.M., Leonard, V.H., Navaratnarajah, C.K., Frenzke, M., Wong, X.X., Sawatsky, B., Ramachandran, S., McCray Jr., P.B., Cichutek, K., von Messling, V., Lopez, M., Cattaneo, R., 2011. Adherens junction protein nectin-4 is the epithelial receptor for measles virus. Nature 480, 530–533.

Nakatsu, Y., Takeda, M., Ohno, S., Shirogane, Y., Iwasaki, M., Yanagi, Y., 2008. Measles virus circumvents the host interferon response by different actions of the C and V proteins. J. Virol. 82, 8296–8306.

Norrby, E., Appel, M.J., 1980. Humoral immunity to canine distemper after immunization of dogs with inactivated and live measles virus. Arch. Virol. 66, 169–177.

Noyce, R.S., Bondre, D.G., Ha, M.N., Lin, L.T., Sisson, G., Tsao, M.S., Richardson, C.D., 2011. Tumor cell marker PVRL4 (nectin 4) is an epithelial cell receptor for measles virus. PLoS Pathog. 7, e1002240.

Ono, N., Tatsuo, H., Hidaka, Y., Aoki, T., Minagawa, H., Yanagi, Y., 2001. Measles viruses on throat swabs from measles patients use signaling lymphocytic activation molecule (CDw150) but not CD46 as a cellular receptor. J. Virol. 75, 4399–4401.

Orvell, C., Norrby, E., 1980. Immunological relationships between homologous structural polypeptides of measles and canine distemper virus. J. Gen. Virol. 50, 231–245.

Osterhaus, A.D., Groen, J., De Vries, P., UytdeHaag, F.G., Klingeborn, B., Zarnke, R., 1988. Canine distemper virus in seals. Nature 335, 403–404.

Perpinan, D., Ramis, A., Tomas, A., Carpintero, E., Bargallo, F., 2008. Outbreak of canine distemper in domestic ferrets (Mustela putorius furo). Vet. Rec. 163, 246–250.

Pratakpiriya, W., Seki, F., Otsuki, N., Sakai, K., Fukuhara, H., Katamoto, H., Hirai, T., Maenaka, K., Techangamsuwan, S., Lan, N.T., Takeda, M., Yamaguchi, R., 2012. Nectin4 is an epithelial cell receptor for canine distemper virus and involved in the neurovirulence. J. Virol..

Qiu, W., Zheng, Y., Zhang, S., Fan, Q., Liu, H., Zhang, F., Wang, W., Liao, G., Hu, R., 2011. Canine distemper outbreak in rhesus monkeys, China. Emerg Infect Diseases 17, 1541–1543.

Roelke-Parker, M.E., Munson, L., Packer, C., Kock, R., Cleaveland, S., Carpenter, M., O'Brien, S.J., Pospischil, A., Hofmann-Lehmann, R., Lutz, H., Mwamengele, G.L., Mgasa, M.N., Machange, G.A., Summers, B.A., Appel, M.J., 1996. A canine distemper virus epidemic in Serengeti lions (Panthera leo). Nature 379, 441–445.

Roscoe, D.E., 1993. Epizootiology of canine distemper in New Jersey raccoons. J. Wildl. Dis. 29, 390–395.

Rothlisberger, A., Wiener, D., Schweizer, M., Peterhans, E., Zurbriggen, A., Plattet, P., 2010. Two domains of the V protein of virulent canine distemper virus selectively inhibit STAT1 and STAT2 nuclear import. J. Virol. 84, 6328–6343.

Sawatsky, B., Delpeut, S., von Messling, V., 2011. Canine distemper virus. In: Samal, S.K. (Ed.), The Biology of Paramyxoviruses. Caister Academic Press, Norfolk, pp. 275–291.

Seki, F., Ono, N., Yamaguchi, R., Yanagi, Y., 2003. Efficient isolation of wild strains of canine distemper virus in Vero cells expressing canine SLAM (CD150) and their adaptability to marmoset B95a cells. J. Virol. 77, 9943–9950.

Seki, F., Yamada, K., Nakatsu, Y., Okamura, K., Yanagi, Y., Nakayama, T., Komase, K., Takeda, M., 2011. The si strain of measles virus derived from a patient with subacute sclerosing panencephalitis possesses typical genome alterations and unique amino Acid changes that modulate receptor specificity and reduce membrane fusion activity. J. Virol. 85, 11871–11882.

Shirogane, Y., Takeda, M., Tahara, M., Ikegame, S., Nakamura, T., Yanagi, Y., 2010. Epithelial-mesenchymal transition abolishes the susceptibility of polarized epithelial cell lines to measles virus. J. Biol. Chem. 285, 20882–20890.

Stephenson, J.R., ter Meulen, V., 1979. Antigenic relationships between measles and canine distemper viruses: comparison of immune response in animals and humans to individual virus-specific polypeptides. Proc. Nat. Acad. Sci. U.S.A. 76, 6601–6605.

Sun, Z., Li, A., Ye, H., Shi, Y., Hu, Z., Zeng, L., 2010. Natural infection with canine distemper virus in hand-feeding Rhesus monkeys in China. Veterinary microbiology 141, 374–378.

Tahara, M., Takeda, M., Yanagi, Y., 2005. Contributions of matrix and large protein genes of the measles virus Edmonston strain to growth in cultured cells as revealed by recombinant viruses. J. Virol. 79, 15218–15225.

Tahara, M., Takeda, M., Yanagi, Y., 2007. Altered interaction of the matrix protein with the cytoplasmic tail of hemagglutinin modulates measles virus growth by affecting virus assembly and cell-cell fusion. J. Virol., 81.

Takeda, M., Kato, A., Kobune, F., Sakata, H., Li, Y., Shioda, T., Sakai, Y., Asakawa, M., Nagai, Y., 1998. Measles virus attenuation associated with transcriptional impediment and a few amino acid changes in the polymerase and accessory proteins. J. Virol. 72, 8690–8696.

Takeda, M., Tahara, M., Hashiguchi, T., Sato, T.A., Jinnouchi, F., Ueki, S., Ohno, S., Yanagi, Y., 2007. A human lung carcinoma cell line supports efficient measles virus growth and syncytium formation via a SLAM- and CD46-independent mechanism. J. Virol. 81, 12091–12096.

Takeda, M., Tahara, M., Nagata, N., Seki, F., 2011. Wild-type measles virus is intrinsically dual-tropic. Front. Microbiol. 2, 279.

Takeuchi, K., Miyajima, N., Kobune, F., Tashiro, M., 2000. Comparative nucleotide sequence analysis of the entire genomes of B95a cell-isolated and Vero cell-isolated measles viruses from the same patient. Virus Genes 20, 253–257.

Tatsuo, H., Ono, N., Tanaka, K., Yanagi, Y., 2000. SLAM (CDw150) is a cellular receptor for measles virus. Nature 406, 893–897.